Chem Soc Rev

REVIEW ARTICLE

Check for updates

Cite this: *Chem. Soc. Rev.*, 2021, **50**, 2074

Self-assembly of colloidal inorganic nanocrystals: nanoscale forces, emergent properties and applications

Xiyan Li,*[a] Xiaowang Liu*[b] and Xiaogang Liu*[cde]

Received 24th April 2020

DOI: 10.1039/d0cs00436g

rsc.li/chem-soc-rev

The self-assembly of colloidal nanoparticles has made it possible to bridge the nanoscopic and macroscopic worlds and to make complex nanostructures. The nanoparticle-mediated assembly enables many potential applications, from biodetection and nanomedicine to optoelectronic devices. Properties of assembled materials are determined not only by the nature of nanoparticle building blocks, but also by spatial positions of nanoparticles within the assemblies. A deep understanding of nanoscale interactions between nanoparticles is a prerequisite to controlling nanoparticle arrangement during assembly. In this review, we present an overview of interparticle interactions governing their assembly in a liquid phase. Considerable attention is devoted to examples that illustrate nanoparticle assembly into ordered superstructures using different types of building blocks, including plasmonic nanoparticles, magnetic nanoparticles, lanthanide-doped nanophosphors, and quantum dots. We also cover the physicochemical properties of nanoparticle ensembles, especially those arising from particle coupling effects. We further discuss future research directions and challenges in controlling self-assembly at a level of precision that is most crucial to technology development.

[a] *Institute of Photoelectronic Thin Film Devices and Technology, Nankai University, Tianjin 300071, China. E-mail: xiyan.li@nankai.edu.cn*
[b] *Frontiers Science Center for Flexible Electronics (FSCFE), MIIT Key Laboratory of Flexible Electronics (KLoFE), Shaanxi Institute of Flexible Electronics (SIFE), 8. Institute of Flexible Electronics (IFE), Northwestern Polytechnical University (NPU), 127 West Youyi Road, Xi'an 710072, China. E-mail: iamxwliu@nwpu.edu.cn*
[c] *Department of Chemistry, Faculty of Science, National University of Singapore, 3 Science Drive 3, 117543, Singapore. E-mail: chmlx@nus.edu.sg*
[d] *Joint School of National University of Singapore and Tianjin University International Campus of Tianjin University, Fuzhou 350207, China*
[e] *The N.1 Institute for Health, National University of Singapore, 117456, Singapore*

Xiyan Li

Xiyan Li received her PhD degree from Changchun Institute of Applied Chemistry, Chinese Academy of Sciences in 2013 under the supervision of Professor Hongjie Zhang. She then worked as a post-doctoral fellow at National University of Singapore and the University of Toronto. She is a professor at the College of Electronic Information and Optical Engineering, Nankai University, China. Her current research focuses on the controlled synthesis, novel properties and optoelectronic applications of semiconductor nanostructures, especially group II–VI semiconductor nanostructure-based optoelectronic devices.

Xiaowang Liu

Xiaowang Liu was born in Anhui, China. He obtained his BS (2004), and MS (2007, under the supervision of Prof. Baoyou Geng) degrees in Physical Chemistry from Anhui Normal University, and PhD degree in Inorganic Chemistry from National University of Singapore under the direction of Prof. Xiaogang Liu. After working as a research scientist (with Prof. Francesco Stellacci) at Institute of Materials, École Polytechnique Fédérale de Lausanne (EPFL), he started his new career at Northwestern Polytechnical University (NPU) as a Professor. His research interests include flexible electronics and controlled assembly of optical nanocrystals.

1. Introduction

Self-assembly is a ubiquitous phenomenon in nature. This process is characterized by a spontaneous organization of discrete building blocks into highly ordered superstructures. Typical examples include the formation of quaternary membrane structures with lipids and protein synthesis on ribosomes.[1–4] Self-assembled superstructures exhibit specific functionality and serve indispensable functions in regulating metabolism. A laudable goal for researchers in biology, chemistry, and neurosciences involves understanding how nature accomplishes self-assembly in complex systems, in order to apply similar techniques in completely different contexts.[5–9] Moreover, owing to large differences in the properties of biomolecules and nanoparticles, the emergence of complex nanoparticle superstructures with unusual properties can meet many technological needs, such as photovoltaics and energy storage devices.[10–13]

Advances in nanoparticle synthesis offer versatility in building-block selections, in terms of size, shape, and composition, for ordered nanoparticle superstructures.[14,15] Understanding nanoscale interaction forces in a liquid phase can be greatly facilitated using particles of uniform size and shape.[5,16] Knowledge of interparticle interactions underpins rational control over nanoparticle self-assembly and facilitates the construction of superstructures suitable for wide applications, including molecule sensing, tandem catalysis, high-density data storage, and optoelectronic devices.[17–22]

Interparticle interactions at nanoscale include van der Waals attraction, electrostatic and steric forces, molecule-dipole effect, hydrogen bonding, depletion, and capillary action. In this review, we start with a brief introduction to types of nanoscale forces, emphasizing key mechanisms that control self-assembly of nanoparticles. We then discuss self-assembly strategies for preparing nanoparticle superstructures.

Xiaogang Liu

Xiaogang Liu received his BE degree in Chemical Engineering from Beijing Technology and Business University, China. He received his MS degree in Chemistry from East Carolina University and completed his PhD at Northwestern University. He then carried out postdoctoral work at MIT for two years before joining the National University of Singapore in 2006. Currently, he sits as an Associate Editor for Nanoscale and serves on the editorial boards of Research, Chemistry – An Asian Journal, Advanced Optical Materials, Journal of Luminescence, and Journal of Physical Chemistry Letters. His research encompasses areas including nanostructured catalysis, optical nanomaterials, optogenetic neuromodulation, and X-ray imaging.

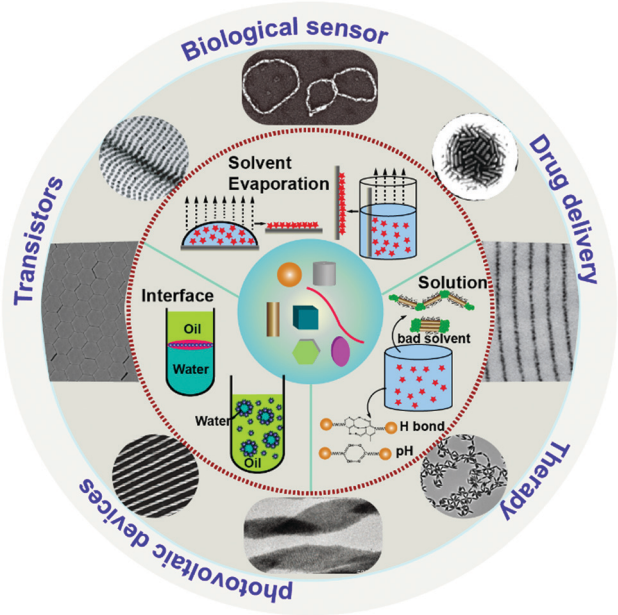

Fig. 1 Schematic illustration of strategies used for self-assembly. Self-assembly studies usually involve three steps: (i) preparation of uniform nanosized building blocks, such as spherical particles, cubes, plates, rods, and wires; (ii) spatially controlled arrangement of these nanoparticles on the basis of competition of multiple nanoscale forces; (iii) exploring potential applications of the assemblies for biological sensing, drug delivery, therapeutics, and energy conversion devices.

Furthermore, we highlight recent advances in nanoparticle-ensemble-based self-assembly and associated properties resulting from interparticle interactions (Fig. 1). The relevance of this emergent field is discussed in terms of recent applications in biomolecule sensing, drug delivery, and energy conversion. Adopting a multidisciplinary research approach is necessary for a better understanding of interparticle interaction principles and extended applications of assembled nanoparticles.

2. Nanoscale forces

Self-assembly of nanoparticles is an important type of aggregation in which thermodynamics or other constraints induce spontaneous organization of nanoparticle building blocks into ordered, macroscopic structures. Aggregation behavior is an outcome of competition between multiple nanoscale forces, including van der Waals forces, electrostatic effects, steric repulsion, molecular dipole interactions, and hydrogen bonding (Fig. 2).[23] In addition, depletion attraction and capillary forces may also come into play, especially during solvent evaporation in the presence of additives.[24]

2.1 van der Waals forces

van der Waals forces arise between isolated atoms, molecules, and even surfaces as a result of fluctuations of electronic clouds within individual components. They exist in all molecules and particles and include three forms of interactions, such as dipole–dipole interactions or Keesom forces, induction or Debye forces, and London dispersion forces.[25] Dipole–dipole

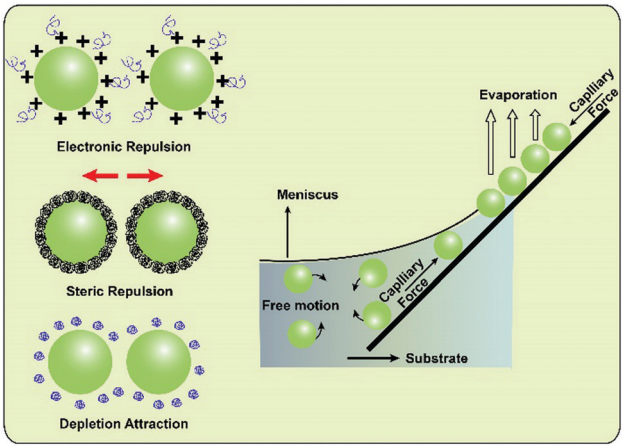

Fig. 2 Schematic illustration of four major types of nanoscale forces, including electronic effects, steric repulsion, depletion, and capillary attraction.

interaction involves electrostatic attractive or repulsive interactions between two polarized molecules due to the inherent difference in their charge distributions.[26] Induction forces involve charged or polar molecules with permanent dipoles that induce charge redistribution on neighboring molecules with no dipole moments. London dispersion forces are the weakest intermolecular force arising in molecules without permanent dipoles. Fluctuations of electron clouds induce temporary changes in charge distribution and instantaneous multipoles in adjacent molecules.[27] Notably, London dispersion forces between nanoparticles do not extend over long distances, and their strength depends on a set of parameters, including chemical composition, shape, and geometry of interacting nanoparticles, as well as interparticle distances. van der Waals forces between nanoparticles can be estimated by a simple pairwise summation method. In this method, the forces are considered as summation interactions of atom pairs located within the two particles. Pairwise results can be expressed by eqn (1):

$$U_{\mathrm{vdW}}(d) = \frac{C_{\mathrm{vdW}}\pi^2}{3n_1n_2}\left[\frac{r_1r_2}{d^2-(r_1+r_2)^2}+\frac{r_1r_2}{d^2-(r_1-r_2)^2} + \frac{1}{2}\ln\left(\frac{d^2-(r_1+r_2)^2}{d^2-(r_1-r_2)^2}\right)\right] \quad (1)$$

where n is the number of atoms per unit volume in the two interacting particles, C_{vdW} is a constant describing the interacting species and the surrounding medium, r_1 and r_2 are the diameters of the two particles, and d is the distance between two particles. Notably, the abovementioned equation is only suitable for evaluating van der Waals forces between two isotropic nanoparticles. In the case of non-spherical nanoparticles, van der Waals forces may become anisotropic due to the presence of non-homogenous distributions of Coulomb repulsion. For example, rod-shaped nanoparticles tend to pack densely side-by-side during drying-mediated assembly. This arrangement occurs because side-by-side attraction interactions are stronger than end-to-end interactions.[28] In essence, van der Waals forces between pairs and groups of adjacent nanoparticles are mostly attractive and non-negligible. For example, van der Waals forces have been demonstrated to account for the synthesis of a three-dimensional (3D) MnO_2 framework through the use of an ice-templating approach.[29] In this study, the birth and growth of ice crystals allow MnO_2 nanoparticles to be squeezed close to one another, significantly increasing van der Waals interactions. The strength is typically one to two orders of magnitude higher than thermal energy (k_BT).[30] However, they become repulsive when the environment's dielectric constant falls between that of the two nanoparticles in solution.[27]

2.2 Electrostatic force

Electrostatic forces are either attractive or repulsive interactions between neighboring particles. For nanoparticles, interaction strength is governed by three factors: potential energy contribution, entropic contribution, and the change in chemical potential energy.[31] Its value can be estimated by eqn (2):

$$U_{\mathrm{es}} = \frac{\varepsilon_0}{2}\int_v (E\cdot D)\mathrm{d}v = \frac{1}{2}\int_A \sigma\varphi_0\mathrm{d}A + \frac{1}{2}\int_V \rho\varphi\mathrm{d}v \quad (2)$$

where ε_0 is the dielectric constant, E is the electric field, and D is the electric displacement. Electrostatic interactions are easily influenced by pH, electrolyte and ion strength, due to screening effects of the charge on nanoparticle surfaces.[32–34] In some cases, an additive can lead to aggregation of nanoparticles in solution. For example, Grzybowski and co-workers reported the formation of loosely packed, diamond-like crystals *via* co-assembly of positively charged Ag nanoparticles and negatively charged Au nanoparticles.[35] In addition to nanoparticles, other additives such as DNA strands also mediate assemblies owing to their strong electrostatic and coordination interactions with diverse nanoparticles.[36]

2.3 Steric force

Steric hindrance usually refers to the repulsive force that occurs between two neighboring nanoparticles coated with polymers or small molecules. When ligand-protected nanoparticles approach each other, the interpenetration of surface ligands can lead to solvent molecule displacement and increased surface free energy. The strength of steric repulsion depends on a set of factors, including ligand density, ligand molecular weight, and ligand solubility in a given solvent. The steric effect can significantly improve the stability of nanoparticle dispersions.[37] Controlling ligand density on the surface of two interacting particles presents a practical means to regulate steric interactions for non-ionic ligand-protected nanoparticles.[38,39] In addition, steric repulsive forces can empower nanoparticles to resist attractive interactions intrinsically and to maintain colloidal stability.[40] For example, a steric polymer layer imparts long-term colloidal stability to ferromagnetic cobalt nanoparticles in a wide range of organic solvents, despite the presence of attractive magnetic forces between the nanoparticles.[41]

2.4 Dipole–dipole interactions

Dipole–dipole interactions occur when two dipolar molecules interact with one another through space. Dipole moments can exist on nanoparticle surfaces because of the noncentrosymmetric distribution of surface charges. Let us consider nonlocal dipoles as two opposite point charges on opposite sides of a nanoparticle. Nanoscale dipole–dipole interactions can be described by Coulomb's law using eqn (3).

$$V_{mn}^{C} = \frac{q_m q_n}{4\pi\varepsilon_0 \varepsilon r_{mn}} \quad (3)$$

where r_{mn} is the distance between the two point charges, m and n. q_m and q_n represent the magnitude of charges on opposite ends of the nanoparticle, ε_0 is vacuum permittivity, and ε is the dielectric constant of the particle's surface.[42] In addition to intrinsic dipole moments of nanoparticles, modifications of molecules with permanent electric dipole moments can also contribute to dipole–dipole interactions. In some cases, this energy is adequate to drive nanoparticle self-assembly. Electric dipoles of gold nanoparticles could be induced by coating them with azobenzene molecules in *cis*-isomer form.[43] Molecular dipole–dipole interactions are tunable using a beam of light, providing a useful strategy for controlling assembly and disassembly of gold nanoparticles.

2.5 Hydrogen bonding interactions

Hydrogen bonding interactions usually occur when a hydrogen atom bonded to an electronegative atom approaches a nearby electronegative atom. A single hydrogen bond is weaker than an ionic bond (or covalent bond), but slightly stronger than van der Waals forces. Typical hydrogen bonds have energies of 2–10 k_BT, depending on the nature of the solvent.[44,45] The strength of hydrogen bonding interactions between nanoparticles is determined by the density of surface anchoring groups (–OH, –COOH or $–NH_2$). In certain instances, these groups can form islands on nanoparticle surfaces.[46] Sun *et al.* demonstrated that hydrogen bonding could be harnessed to regulate pH-dependent reversible assembly and disassembly of Au nanorods for many cycles.[47] In a separate study, Etgar *et al.* developed a simple toolbox to couple PbSe nanocrystals with superparamagnetic γ-Fe_2O_3 nanoparticles by taking advantage of hydrogen bonding interactions.[48] To test the approach, the researchers coated PbSe nanocrystals with NH_3^+ groups and γ-Fe_2O_3 nanoparticles with polyhedral silsesquioxane ligands. The functionalization of magnetic nanoparticles with luminescent quantum dots yielded a hybrid system with dual functions of luminescence for imaging and carrier capability for drug delivery.

2.6 Depletion attraction

In a dispersion of large and small particles, depletion force is an attractive force between large particles and arises from increased osmotic pressure of the surrounding solution. The depletion attraction results from an entropic effect, that is, the overlap of the bound volumes of large particles gives rise to more volumes accessible by small particles. In a colloidal system, nanoparticles are treated as large particles, whereas small particles refer to additives, such as solutes and molecules.[49,50] When large nanoparticles approach each other nearby, additives cannot enter spaces between nanoparticles due to a size mismatch. Under such conditions, osmotic pressure triggers formation of particle aggregates. The magnitude of the depletion force is on the order of 4–12 k_BT, capable of inducing assembly of colloidal particles with relatively low curvature, such as nanorods or nanocubes.[51–53] For instance, the depletion force has been harnessed to guide assembly of CdSe/CdS nanorods into close-packed, hexagonally ordered monolayer arrays.[49]

2.7 Capillary force

Capillary force is a special type of interaction acting on particles through fluid interfaces. This attractive force arises from the overlap of menisci formed around separate particles. The effect, which can be attractive or repulsive, can cause aggregation and ordering of particles on a rather wide length scale. Well-ordered 2D arrays of nanoparticles or submicrometer particles tend to form on surfaces of desirable substrates through dip coating. This process involves immersing the substrate in a precursor solution and then lifting it vertically out of the solution at a controlled speed. The magnitude of capillary action is about 100 k_BT. Such a force is strong enough to enable side-by-side alignment of anisotropic nanoparticles, such as CdS nanorods, into ordered 2D or 3D assemblies by elegant control of solvent evaporation from their concentrated dispersion.[54]

3. Self-assembly involving multi-type nanoparticles

With rapid developments in inorganic nanoparticle synthesis, electronic, optical, and magnetic properties of nanoparticles can be precisely modulated by harnessing quantum confinement effects. These physical properties are also sensitive to the coupling effect provided by neighboring similar or dissimilar building blocks. Precise control over nanoscale forces regulates self-organization of adjacent nanoparticles, thus allowing predesigned nanoparticle superstructures to be constructed. This ability not only adds flexibility to produce assemblies with desirable properties, but also provides insight into physical origins of coupling effects.

According to differences in spatial arrangements of building blocks, nanoparticle assemblies, in general, can be divided into two classes: those with periodic or quasi-periodic ordered superstructure and short-range polymeric nanoparticles. In this section, we summarize the self-assembly of a diversity of nanoparticles into long- or short-range ordered assemblies, based on collective interactions of the nanoscale forces mentioned above. Due to space limitations, we will focus on the following four nanoscale building blocks: plasmonic nanoparticles, quantum dots, magnetic nanoparticles, and lanthanide-based nanoparticles.

3.1 Plasmonic nanoparticles

Advances in colloidal synthetic chemistry benefit plasmonic nanoparticle synthesis (*e.g.*, Au and Ag) with controlled morphology, such as spheres, rods, wires, plates, polyhedrons, pyramids, and branched-shaped particles.[55] Tailorable plasmonic properties of these nanoparticles make it possible to customize them for specific applications.[56] Also, thiol chains of various lengths have been used to cover noble metal surfaces, effectively rendering metal nanoparticles inert to oxidation and ideal for facet-specific functionalization. This ability allows control over multiple nanoscale forces affecting nanoparticles. Taken together, these factors underpin remarkable development in driving nanoscopic self-assembly of plasmonic nanoparticles for widespread applications.[17,57,58] In this section, we review self-assembly of plasmonic nanoparticles with particular emphasis on nanoscale-specific interparticle forces.

Depletion attraction plays a vital role in regulating Au nanoparticle assemblies. One of the earliest examples was demonstrated by Kumacheva and co-workers, who carried out controlled self-assembly of Au nanorods by changing water content in organic solvents.[59] To achieve this, the researchers first modified Au nanorods with CTAB (cetyltrimethylammonium bromide) on their sides and polystyrene (PS) ligands on their ends. By elegantly controlling the level of osmotic pressure, the as-modified Au nanorods could be assembled into rings, nanochains, bundles, and nanospheres (Fig. 3). In addition, other morphologies such as vesicles, rafts, dimers, trimers, and frameworks are possible using similar strategies.[53] The limitation of this strategy lies in the fact that binary ligand distribution on nanoparticle surfaces needs to be precisely controlled because the relative volumes of hydrophobic-to-hydrophilic domains and relative interactions of the two domains with solvent molecules play a pivotal role in determing the size and shape of resulting aggregates. Currently, such a control over the ligand distribution only limits to noble nanoparticles that promote facet-specific bonding of thiol groups to nanoparticle surfaces.

Electrostatic interaction provides a valuable tool to control self-assembly of metal nanoparticles, especially for those capped with ionic molecules or polymers. The utility of electrostatic interaction-based strategies is based on adjusting the strength of attraction by controlling ionization and deionization of surface ligands. Xia *et al.* reported reversible self-assembly of Au nanoparticles capped with a pH-sensitive ligand, poly([2-(dimethylamino)ethyl]methacrylate) (PMDA).[60] In this study, protonation of surface-tethered polymers gradually reduced interparticle electrostatic repulsion. As a result, the average number of Au nanoparticles in each chain assembly could be varied between 2 and 8.

Changes in precursor solution, such as pH, may also alter intermolecular hydrogen bonding. The dual actions of electrostatic and intermolecular interactions allow 1D nanoparticle chains to form. Sun *et al.* demonstrated the feasibility of using mercaptopropionic acid-modified Au nanorods for end-to-end nanorod assembly.[47] To achieve this feat, the authors needed to increase the pH of the colloidal solution above the isoelectric point. By comparison, Au nanorods capped with mercaptoundecanoic acid yielded a mixture of products *via* end-on or side-on attachment, which could be attributed to poor facet selectivity of the capping molecule.[46,61]

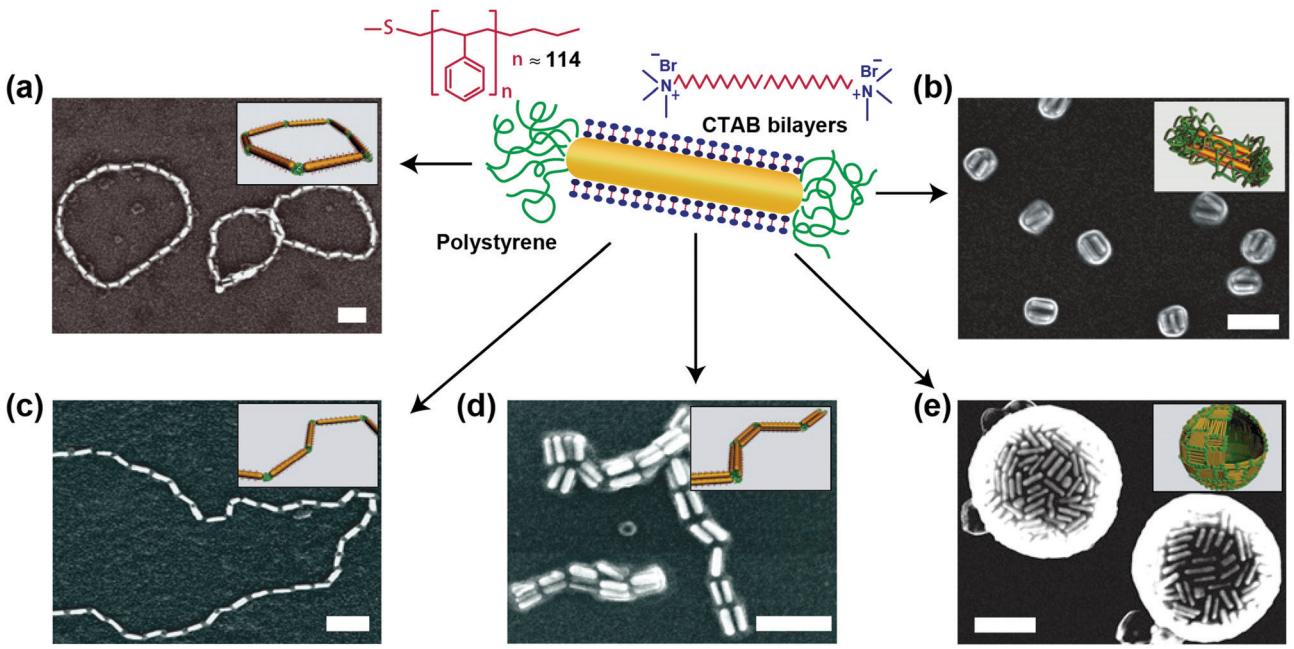

Fig. 3 Self-assembly of polymer-tethered Au nanorods in mixed solvents. The building blocks of Au nanorods were modified with CTAB (cetyltrimethylammonium bromide) along their sides and polystyrene molecules at their ends. SEM images of self-assembled nanorod structures: (a) rings, (b) aggregated nanorod bundles, (c) chains, (d) bundled nanorod chains, (e) nanorod nanospheres. Scale bars are 100 nm. Insets show corresponding schematic diagrams of nanorod assemblies. (Reproduced with permission from ref. 59, copyright 2007, Nature Publishing Group.)

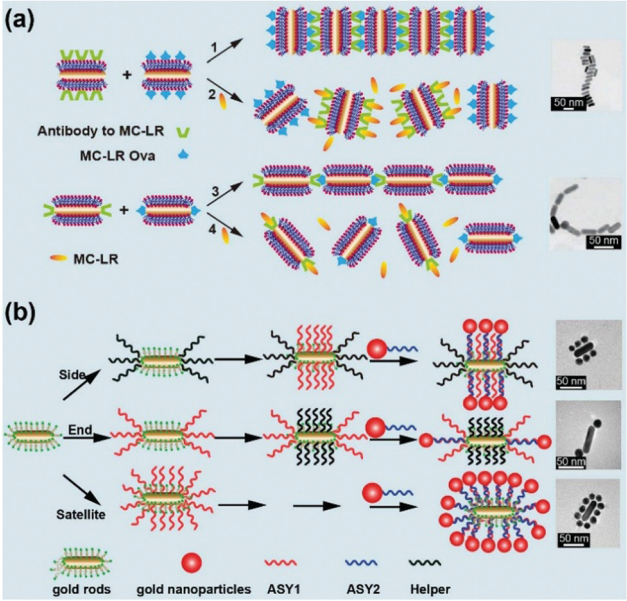

Fig. 4 (a) Schematics of toxin detection *via* using side-by-side and end-to-end Au nanorod assemblies. Insets show representative TEM images. (b) Schematics of formation of regiospecific Au nanoparticle assemblies. Insets show representative TEM images of end-, side-, and satellite-assemblies, respectively. (Reproduced with permission from ref. 62 and 68, copyright 2010, Wiley-VCH Verlag GmbH & Co. KGaA, and copyright 2011, American Chemical Society.)

Compared with intermolecular hydrogen bonding, biomolecular recognition, such as antibody–antigen interaction and sequence-specific DNA hybridization, can achieve more specific binding of plasmonic nanoparticles during assembly. There is strong evidence that the high selectivity of biomolecular recognition enables robust analytical platforms for molecular detection. Kotov's group explored unique optical properties of Au nanorod assemblies for ultrasensitive and selective sensing of environmental toxins (Fig. 4a).[62] The researchers found that it was possible to control Au nanorod assemblies through side-on or end-on attachment by surface antibody coating and the optimization of antibody–antigen interactions. A challenging issue of this strategy for practical utilization is how to control antibody–antigen interactions site-specifically at the ends of nanorods. This would provide improved sensitivity due to enhanced surface plasmon resonance in the presence of the analyte.

Through judicious selection of plasmonic nanoparticles and DNA linkers with specific sequences, one can control spacing and periodicity of nanoparticle building blocks within a macroscopic or polymeric structure. Typical morphologies include multimeric network, chiral pyramid, chain, 2D and 3D superstructures.[63–68] Xu *et al.* innovatively used DNA oligomers to study complex assemblies of Au nanoparticles and nanorods (Fig. 4b).[68] Their work revealed distinct regiospecificity resulting from anisotropic interactions of the constituents. Based on three types of assembled structures formed (end, side, and satellite isomers), the researchers presented the first proof-of-concept, real-time probing of the local organelle environment in living cells.

Notably, achieving spatially controlled arrangement requires not only sequence-specific DNA hybridization, but also facet-selective DNA modification of Au nanorods. An exemplary work on chiral pyramid synthesis was reported by Alivisatos *et al.*, who modified four sizes of Au nanoparticles with distinct, but complementary single-stranded DNA sequences and then performed DNA hybridization (Fig. 5a).[69] This strategy also endows superlattices with great flexibility in stoichiometry control. In a parallel development, Gang and co-workers reported that Au nanorods, modified with flexible DNA chains along their sides, could undergo head-to-head arrangement to yield 1D ladder-like ribbons (Fig. 5b).[70]

As an added benefit, DNA-mediated assembly allows one to switch nanoparticle assembly configuration by changing the environmental conditions.[71] Transformation of hexagonally ordered 2D Au nanoparticle arrays to a weakly ordered network has been accomplished by Gang and co-workers.[72] They found that DNA complementarity upon increasing ionic strength is an essential factor affecting electrostatic repulsion between negatively charged Au nanoparticles (Fig. 5c). Rigid DNA scaffolds are ideal templates for controlling the 3D arrangement of Au nanoparticles. For example, DNA origami was utilized by Liedl's group to construct plasmonic nanohelices that display circular dichroism and optical rotatory dispersion effects in solutions (Fig. 5d).[73]

Functionalization of metal nanoparticles with DNA strands provides a versatile route toward the assembly of highly ordered nanostructures and hierarchical materials. Despite limitless opportunities, a key challenge to DNA-mediated self-assembly lies in the understanding of the fundamental principle of self-assembly and the structure–property correlation. Computer modeling and molecular simulation techniques may provide a much-needed solution, allowing access to a level of detail that is inaccessible in traditional experimental investigations, mostly because of the high complexity of interactions at nanometer dimensions.

To produce high levels of structural complexity, great efforts should be devoted to high-quality nanoparticle synthesis with delicate control over morphology and surface functionalization. Moreover, new strategies have been developed to impart nanoparticle building blocks with anisotropic regioselectivity. Site-specific functionalization of plasmonic nanoparticles has a special significance because of its ability to control bonding directionality and the coupling strength between nanoparticle building blocks. Access to plasmonic superlattices with tailored size, geometry and composition will promote structure–function relationship studies, important in fields spanning molecular sensing and optoelectronics.

3.2 Quantum dots

Quantum dots are typically semiconducting nanocrystals that possess high photostability, size-dependent emissions, and high extinction coefficients. These features have made quantum dots the material of choice for applications in next-generation optoelectronics and light-emitting display.[74–78] Facile synthesis of quantum dots with various shapes *via* wet

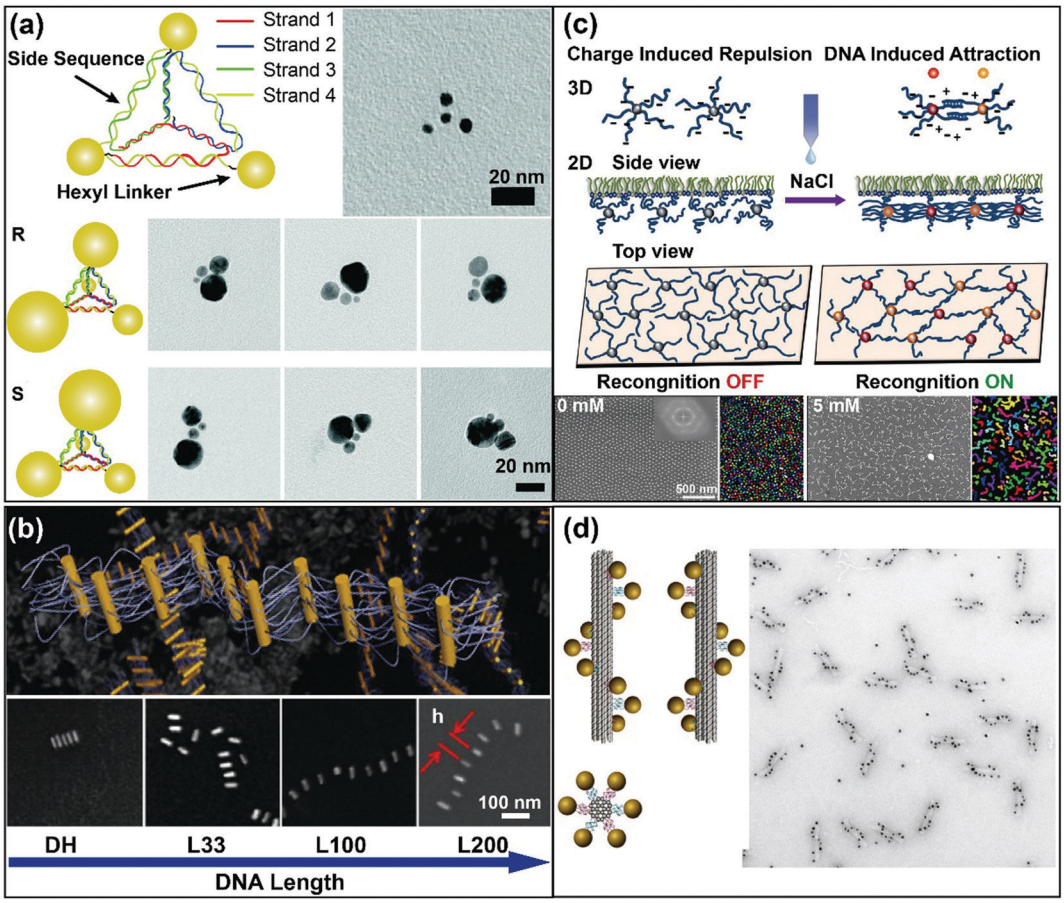

Fig. 5 (a) Schematic illustration of the synthesis of DNA–Au nanocrystal pyramids and their corresponding TEM images. (b) Representative TEM images of ribbon-like nanorod assemblies using thiolated DNA linkers of variable lengths (DH, L33, L100, and L200), showing similar assembly morphologies, but different interparticle spacings. (c) Schematic illustration of the assembly of DNA-functionalized Au nanoparticles at positively charged interfaces. In the absence of salt, the electrostatic repulsion between DNA chains dominates interactions. However, an attractive interaction between nanoparticles was switched on due to DNA hybridization in the presence of monovalent salt. (d) Schematic representation of the assembly of DNA origami gold nanoparticle helices and TEM image of the resulting product. (Reproduced with permission from ref. 69, 70, 72 and 73, copyright 2009, 2013, 2014, and 2012, American Chemical Society, and Nature Publishing Group.)

chemistry adds another dimension in developing self-assembly strategies. The resulting self-assembled structures could be furnished with delocalized charge carriers, increased charge transport, and unique optoelectronic properties.[79–81] These assemblies can reach micrometer sizes through control of conditions under which quantum dots are assembled.[82,83]

3.2.1 Self-organization process in solution. Dipole–dipole interparticle interactions are an important class of nanoscale forces governing self-assembly of quantum dots. This type of interaction not only exists in *in situ* synthesis, but also in post-synthesis.[84–93] For example, Murray and coworkers reported the importance of adjusting dipole–dipole interactions in shape-controlled synthesis of PbSe quantum dot assemblies. These shapes include straight, helical zigzag, helical, branched, and tapered nanowires, as well as single-crystal nanorings. They predicted the largest magnitude of dipole moment along the ⟨100⟩ direction of constituent PbSe nanoparticles, driving oriented attachment and subsequently nanoparticle fusion along the same crystal facets (Fig. 6a).[94] Another interesting development was reported by Tang and co-workers, who achieved self-assembly of CdTe nanocrystals into free-floating particulate sheets. They reported that strong dipole interactions between nanoparticles are the major driving force for the self-organization process leading to a collective state of nanoparticles (Fig. 6b).[95] This work was considered a major revelation regarding the mechanism of superparticle growth that resembles closely assembly of surface layer (S-layer) proteins.

For nanoparticles with uniform size or morphology, self-assembly generally occurs *via* a strong non-equilibrium process and terminates with highly ordered structures. This mechanism is known as self-limiting growth in which a combination of electrostatic repulsion and van der Waals interactions comes into play.[96] Tang, Glotzer, Kotov and colleagues pioneered the self-limiting growth strategy for synthesis of monodisperse CdSe superparticles (Fig. 6c and d).[82] Banin *et al.* reported another excellent demonstration of self-limiting assembly for ZnSe nanorod dimers (Fig. 6e).[93] Nanorods were first prepared by self-assembly and oriented attachment

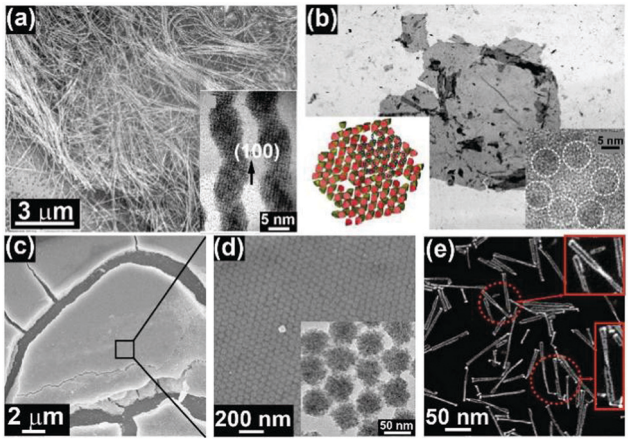

Fig. 6 (a) SEM image of solution-grown PbSe nanowires. The inset shows the corresponding TEM image. (b) TEM image of 2D CdTe nanoparticle superstructures. Left and right insets show a schematic illustration of the nanosheet model and corresponding HRTEM image, respectively. (c and d) SEM images of colloidal CdSe superstructures. The inset in d shows TEM imaging of the superstructures. (e) HAADF-STEM imaging of ZnSe nanorod dimers. (Reproduced with permission from ref. 94, 95, 82 and 93, copyright 2005, 2006, 2011, and 2014, American Chemical Society, American Association for Advancement of Science, and Nature Publishing Group.)

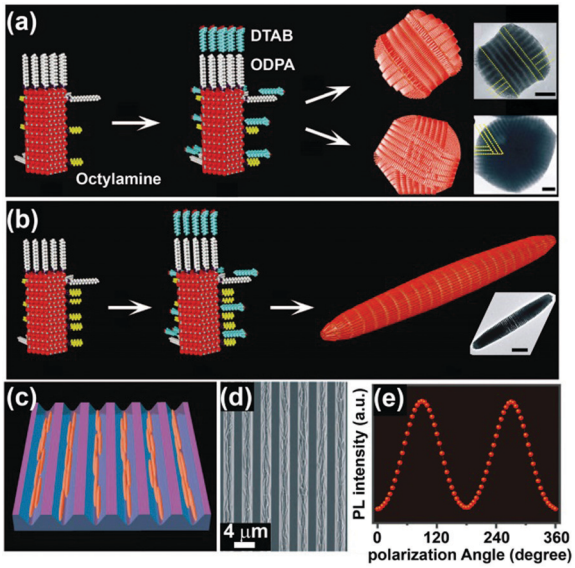

Fig. 7 (a and b) Schematic illustrating the synthesis of cylindrical disks and needle-like superparticles using CdSe/CdS nanorods as building blocks. Insets show TEM images of corresponding superparticles. (c) Schematic representation of a lateral alignment of superparticles into unidirectional line patterns on a solid substrate. (d) SEM image of laterally aligned, needle-like superparticles inside a line-patterned Si_3N_4 substrate. (e) polarization angle-dependent photoluminescence intensity measurement (380 nm excitation). (Reproduced with permission from ref. 100, copyright 2012, American Association for Advancement of Science.)

of individual ZnSe nanoparticles. Optimization of attractive van der Waals forces and charge-pairing interactions then led to loosely bound nanorod pairs. In both cases, products have high structural uniformity comparable to that of cellular adhesion complexes, collagen fibres and viral capsids formed *via* self-assembly of proteins. This structural feature is an outcome of the fact that the driving force, namely van der Waals interaction, is gradually offset through interparticle electrostatic repulsion, allowing the self-assembly process to cease under thermodynamic equilibrium conditions.

3.2.2 Colloidal single-crystalline superparticles. Hydrophobic van der Waals interactions in an aqueous phase between surfactant molecules and capping ligands can result in thermodynamically defined, interdigitated bilayer structures.[97] By harnessing this molecular effect, Li and co-workers demonstrated a general, robust approach to preparing a broad range of superparticles, including CdS, PbS, and Bi_2S_3.[98] Anisotropic interparticle interactions seem to dominate for non-spherical nanoparticles as building blocks. For example, Cao's group reported the growth of hexagonal closely packed superparticles from dodecyl trimethylammonium bromide-capped CdSe/CdS nanorods along the *c*-axis of the nanorods.[99] Introducing repulsive solvophobic interactions between *in situ* formed superparticles and ethylene glycol solvent molecules further transformed the superparticles into round structures (Fig. 7a). In a follow-up study, Cao and colleagues found that anisotropic interactions between CdSe/CdS nanorods could be kinetically introduced during assembly, promoting formation of single-domain, needle-like superparticles with parallel alignment of constituent nanorods.[100,101] Furthermore, these needle-like superstructures could be unidirectionally aligned on a solid, patterned substrate and further transformed into macroscopic freestanding polymer films (Fig. 7b–e). The needle-like superstructures exhibited strong linearly polarized photoluminescence, rendering them potentially suitable as optoelectronic devices, such as light-emitting diodes.

3.2.3 Closed-packed superstructures. Capillary attraction has a profound impact on self-assembly of close-packed semiconductor superstructures through slow solvent evaporation.[102–108] Notably, a set of parameters, such as the nature of the ligand on nanoparticle surfaces, particle shape, solvent evaporation rate, and the substrate of choice, can influence interparticle distances within close-packed superstructures.[109] Interparticle distance affects optical and electronic properties of resultant superstructures as well as the performance of superparticle-based devices.[110–114]

Urban *et al.* reported that solvent nature impacts capillary attraction and subsequently influences the pathway of PbTe nanoparticles to be arranged.[115] In their study, they showed that using trichloroethylene as the solvent densely packed nanocrystal superlattices formed, whereas chloroform resulted in densely packed glassy films. Hanrath *et al.* revealed that nanocrystal–substrate interactions could drive PbSe nanoparticle crystallization and form materials with controlled crystal symmetry, stoichiometry, and dimensionality.[116] In contrast, a plain substrate only yielded polycrystalline aggregates with indistinct crystal boundaries. Although it is relatively straightforward to design systems with good nanocrystal–substrate interactions, growth of close-packed superstructures on different substrates is more challenging. Alivisatos *et al.* highlighted the importance of kinetic control on orientational order and

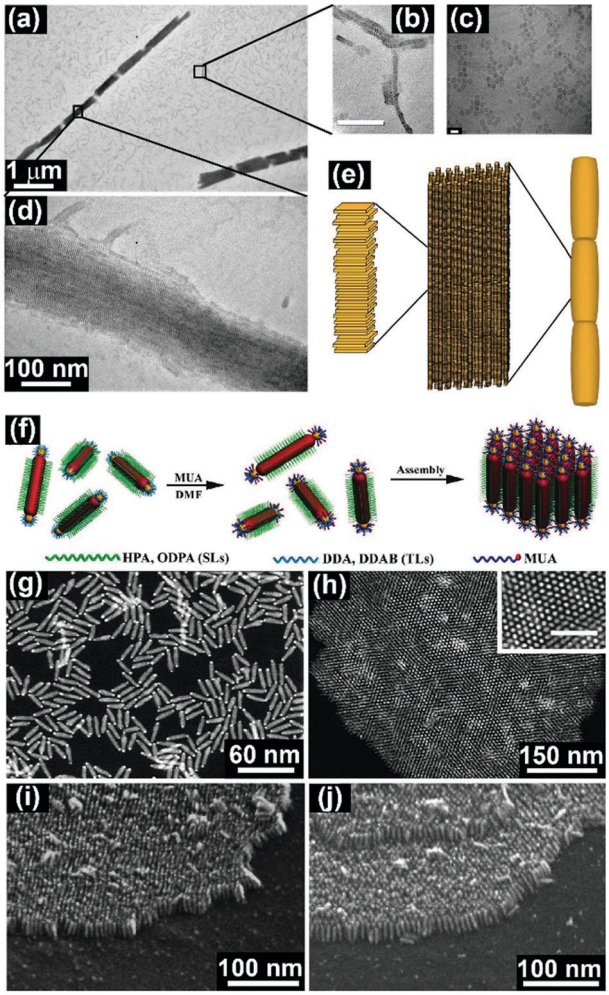

Fig. 8 (a–c) TEM imaging of self-assembly of CdSe nanoplatelet building blocks. Scale bars: 100 and 20 nm for b and c, respectively. (d) High-magnification TEM imaging showing the stacking of nanoplatelets within a superparticle. (e) Schematic illustration of hierarchical structures of superparticles. (f) Schematic representation of the self-assembly of Au-tipped CdSe nanorods. (g and h) TEM images of Au-tipped CdSe nanorods and the close-packed nanorod array. The inset shows a magnified image (scale bar: 50 nm). (i and j) SEM images of nanorod bundles. (Reproduced with permission from ref. 117 and 118, copyright 2013 and 2009, American Chemical Society.)

reported that with gentle heating, unprecedented vertical control (96% per cm^2) over CdS nanorod self-assembly could be achieved on a wide range of substrates such as ITO, PEDOT:PSS, and Si_3N_4.[54]

Mixing a nanoparticle solution with an antisolvent, in which the product is sparingly soluble, may lead to close-packed superparticle supersaturation and solidification. This process is known as antisolvent crystallization. Dubertret and co-workers achieved antisolvent crystallization of micrometer-scale, needle-like superparticles by adding traces of ethanol to a cyclohexane dispersion containing CdSe nanoplatelets (Fig. 8a–e).[117] Highly oriented perpendicular alignment of nanoplatelets rendered the superparticles with polarized light emission properties.[114] This technique was also used for rod-like nanostructure assembly. For example, Kumacheva's group realized side-by-side assembly of Au-tipped CdSe nanorods with a controllable and scalable size distribution (Fig. 8f–j).[118] Hydrogen bonded groups could be introduced to Au tips to improve assembly durability.

While self-assembly of spherical, rod-shaped, and platelet-like nanoparticles has advanced significantly during the past decade, nanoparticle assembly with high geometric complexity has made limited progress due to inadequate structural stability in the absence of orientational order. Morphology-dependent steric restrictions become prominent during self-assembly process.[119–122] Morphological diversity in nanoparticles can help create more complex materials by mimicking molecule-level reactions. Exciting work was reported by Manna and co-workers, who successfully controlled self-assembly of octapod-shaped CdSe/CdS nanocrystals by balancing interparticle van der Waals forces and particle–solvent interactions.[120] They found that the octapod-shaped CdSe/CdS nanoparticles were initially self-organized into linear chains due to the stronger octapod–octapod interactions relative to octapod–solvent interactions (Fig. 9). The chains continued to interact with each other and finally transformed into ordered 3D superstructures in solution.[120] Notably, when depositing on flat substrates to induce nanoparticle–substrate interactions, the octapods preferentially assembled into a 2D square lattice with limited free rotation freedom of the octapod constituents.[123,124]

A major challenge in studies of self-assembly of nonspherical nanoparticles is associated with the difficulty of predicting product morphologies. Shape-anisotropy may dominate the

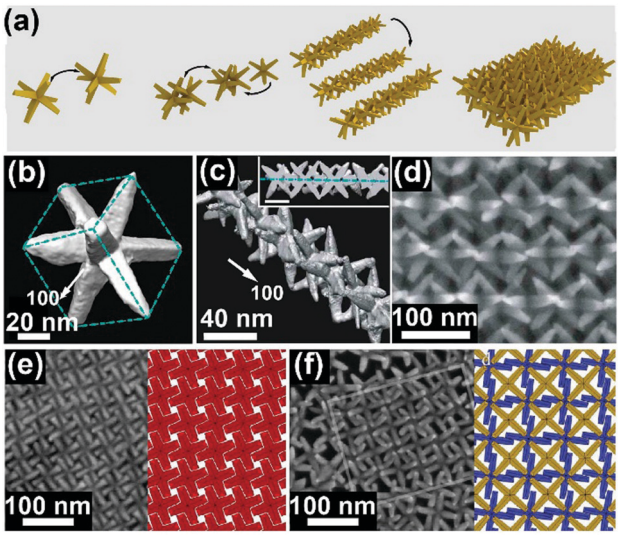

Fig. 9 (a) Schematic synthesis of octapod-shaped CdSe/CdS nanocrystal chains *via* self-assembly. (b and c) 3D images of a single octapod and an assembled octapod chain reconstructed from STEM imaging. (d) A close-view of the nanocrystal assembly. (e and f) TEM images showing simple square lattices and binary square lattices of the samples, obtained *via* solvent evaporation of octapod dispersions. Insets showing simulated patterns of superlattice structures. (Reproduced with permission from ref. 120 and 123, copyright 2011 and 2012, Nature Publishing Group and American Chemical Society.)

self-assembly process either spontaneously or in the presence of an external field. Currently, theoretical simulations only provide limited structural information with energetically more favorable arrangements and are unable to predict kinetically controlled assemblies. For example, the ratio of high-index facet to surface area becomes larger when shape anisotropy of the building blocks increases. Consequently, extra calculation parameters are required to characterize the nature of sub-component interactions dominated by high-index facets. To this regard, one would expect a vast increase in the configurational degrees of freedom of complex nanoparticles, thereby making simulation algorithms challenging.

3.2.4 Binary nanoparticle superlattices. Nanoscale forces that involve self-assembly of nanoparticles of two different sizes into a binary nanoparticle superlattice are much more complicated to characterize.[125] Murray and co-workers led the pioneering effort on strategies for different binary nanocrystal superlattices using various combinations of nanosized building blocks.[106,111,126–128] They found that electrical charges on sterically stabilized nanoparticles determined the stoichiometry of resulting binary nanoparticle superlattices. They developed more than 15 different binary superlattices with various packing symmetries, such as NaCl, CuAu, AlB_2, $MgZn_2$, $MgNi_2$, Cu_3Au, Fe_4C, $CaCu_5$, CaB_6, and $NaZn_{13}$ (Fig. 10).[112,127] Additional interactions, including entropic force, van der Waals, steric, and dipolar effects contributed significantly to stabilization of binary nanoparticle superlattices. As expected, controlling relative molar ratios of nanoparticles provides an additional tool to regulate stoichiometry of superlattices. For example, an increase in component concentration in the mixture transformed the stoichiometry from AB_4 to AB_{13}.[111,129]

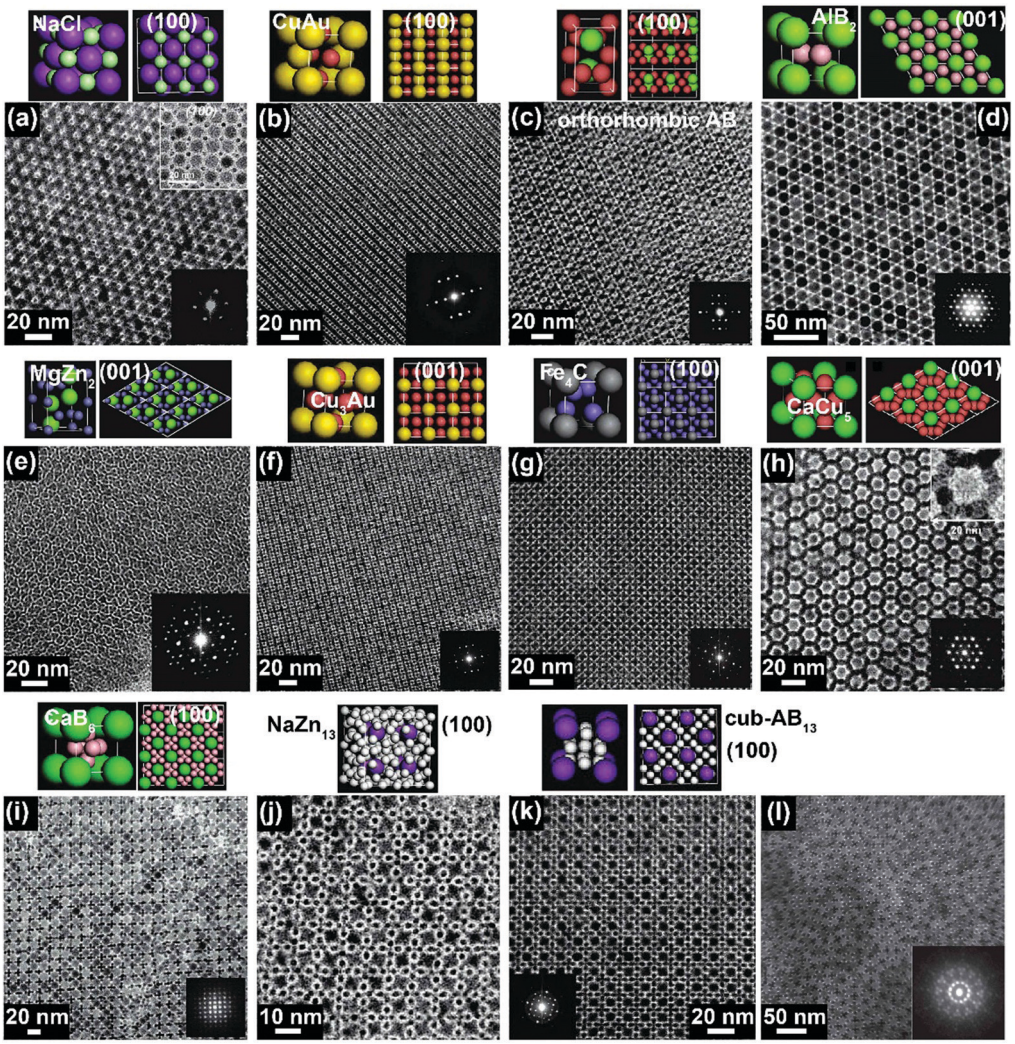

Fig. 10 TEM images of self-assembled binary superlattices from two types of nanoparticles, corresponding unit cell models, and electron diffraction patterns. (a) PbSe (7.2 nm) and Pd (3.0 nm) nanoparticles. (b) PbSe (5.8 nm) and Ag (3.4 nm) nanoparticles. (c) PbSe (5.8 nm) and Pd (3.0 nm) nanoparticles. (d) Fe_2O_3 (13.4 nm) and PbSe (5.8 nm) nanoparticles. (e) PbSe (6.2 nm) and Pd (3.0 nm) nanoparticles. (f) PbSe (5.8 nm) and Ag (3.4 nm) nanoparticles. (g) PbSe (5.8 nm) and Pd (3.0 nm) nanoparticles. (h) PbSe (7.2 nm) and Au (5.0 nm) nanoparticles. (i) Fe_2O_3 (13.4 nm) and Au (5.0 nm) nanoparticles. (j) PbSe (5.8 nm) and Pd (3.0 nm) nanoparticles. (k) PbSe (5.8 nm) and Pd (3.0 nm) nanoparticles. (l) TEM image of a quasicrystalline superlattice self-assembled from Fe_2O_3 (13.4 nm) and Au (5 nm) nanoparticles. (Reproduced with permission from ref. 112 and 127, copyright 2006 and 2009, American Chemical Society and Nature Publishing Group.)

Although exquisite control of interparticle interactions for the synthesis of binary nanoparticle superlattices can be achieved, phase segregation may occur to some extent when there is a marked difference in attractive forces of nanoparticles of different sizes. This leads to the formation of nanoparticle aggregates in addition to binary superlattices, making it impossible to conclusively evaluate structural properties in thin-film or powder forms. Despite the challenges, binary nanoparticle superlattices have the potential to enable a variety of novel, 3D dynamic structures, suitable for exploring the principles of single nanoparticle-based elementary reactions.

3.3 Magnetic nanoparticles

Magnetic nanoparticle assembly depends heavily upon magnetic dipole interactions exerted by individual building blocks. Even without applying an external magnetic field, magnetic nanoparticles tend to align their magnetic dipole moments in a head to tail manner to form a nanoparticle chain or ring-like configuration due to anisotropic magnetic interactions (Fig. 11a).[130–132] Despite the high directionality of magnetic interactions, such assembled patterns are not readily observable using TEM because thermal agitation may destroy assembled structures, especially under weak magnetic interactions.[28] In a simple model where only magnetic nanospheres are considered, the magnitude of magnetic interactions between two magnetic nanospheres can be expressed by eqn (4):

$$\mu = \frac{r^6 M_s^2}{\sigma^3} \tag{4}$$

where r is the radius of magnetic nanoparticles, M_s is the saturation magnetization and σ is the separation distance between two nanoparticles.[133] From eqn (4), nanoparticles with larger diameters favor dipole-induced assembly. For example, Butter *et al.* utilized this principle to study assembly of Fe_3O_4 nanoparticles with sizes from 2 to 8 nm.[134] They found that only nanoparticles larger than 7 nm assembled into chain-like structures. However, for Fe_3O_4 nanoparticles substantially larger than 7 nm, dominant magnetic dipole interactions also led to rapid particle aggregation.

Apart from 1D chain-like structures formed in solution or deposited on substrates,[135,136] monodisperse magnetic nanoparticles can also assemble into 2D or even 3D large-area superlattices by slow evaporation of concentrated magnetic fluid droplets. To obtain such close-packed superstructures, small (<20 nm) nanoparticles with weak magnetic interactions are typically chosen as superlattice building blocks (Fig. 11b).[137,138] However, the use of small, "weak" magnetic building blocks weakens the idea of creating superlattices with strong magnetic responses which are important for applications as high-density magnetic storage materials and permanent magnets. To solve this problem, a controlled post-assembly annealing process is commonly employed to enhance the ferrimagnetism of assembled nanostructure while maintaining the original 2D frameworks.

For magnetic nanoparticle assembly, it is essential to maintain a delicate balance between multiple interactions, including van der Waals forces, electrostatic interactions, and magnetic dipole–dipole interactions. Despite the utility of simulations for self-assembly modeling, experimental details in terms of nanoparticle concentration, surfactant molecules, and solvent evaporation dynamics, to name a few, still require careful tuning. To minimize such complications, an external magnetic field is often applied to provide additional controllability for magnetic nanoparticle assembly.

Upon applying an external magnetic field, magnetic nanoparticles tend to align their magnetic moments in parallel with the external field. In addition, if the applied field is non-uniform in space, magnetic nanoparticles would be driven to places where the local magnetic field reaches its maximum. These two fundamental rules and the rapid response of nanoparticles to external magnetic stimuli provide enormous possibilities for accurately constructing nano-assemblies and for remotely controlling their dynamics with ease.

In the absence of an external magnetic field, magnetic nanoparticles can form nanochains and rings. However, their morphologies and chain lengths are random and unpredictable, preventing reproducible results and utilization for further applications. In contrast, recent works have shown that

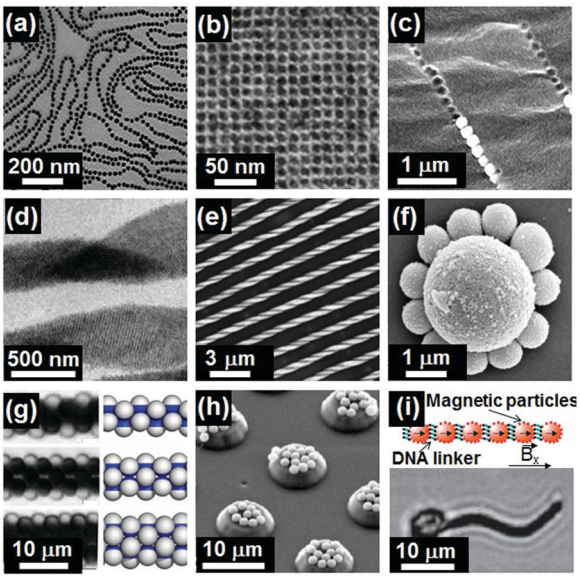

Fig. 11 (a) Nanochains formed from Co nanoparticles in the absence of a magnetic field. (b) 2D superlattices assembled from small Fe_3O_4 nanocubes. (c) Linear Fe_3O_4 chains in a polymer matrix, forming a 1D crystal with unique colors (d) Helical ribbons obtained from Fe_3O_4 nanocubes in the presence of a magnetic field. (e) SEM images of structures (in d) highlighting the same chirality of the assembled structures. (f) "Saturn-rings" assembled from a mixture of paramagnetic particles and non-magnetic particles dispersed in ferrofluid. (g) Microtubes assembled from magnetic Janus colloids with various types of packing. (h) Assembly of non-magnetic particles onto patterned substrates in a ferrofluid environment. (i) One magnetic swimmer that transports a red blood cell under varying magnetic fields. (Reproduced with permission from ref. 132, 138, 143, 147, 148, 150, 152 and 153, copyright 2007, 2007, 2009, 2014, 2009, 2012, 2012, and 2005, American Chemical Society, National Academy of Sciences, USA, Nature Publishing Group, and American Association for Advancement of Science.)

by applying an external magnetic field to a magnetic colloidal solution, nanoparticles assembled into perfect 1D photonic crystals comprising periodically alternating phases of different refractive index.[139,140] The diffractive colors of these photonic crystals are governed by Bragg's law[141,142] and can be tuned by changing the inter-particle distance. Due to their superb stability and fast responsiveness, these magnetic nano-assemblies have been used for smart painting, information display, and magnetic nanomixing (Fig. 11c).[143–146]

In addition to linear assemblies, more complex structures, such as helical, chiral nanobelts (Fig. 11d and e), 3D nano-flowers and Saturn ring-like particles (Fig. 11f), have also been prepared using magnetic nanoparticles.[147,148] To add control over assembled structures, magnetic nanoparticles can be modified into patchy or Janus colloidal motifs using a template before assembly.[149] For example, silica particles with hemi-spherical nickel coatings could lead to various micro-tubular structures that were interchangeable in a predictable manner (Fig. 11g).[150] In another report, Fe_2O_3-containing asymmetric nanoparticles assembled into chiral structures, resembling the chirality typically expected for small asymmetric molecules.[151] It should be noted that the magnetic field-guided strategies are not limited to magnetic nanoparticle building blocks. They can also be extended to non-magnetic components. A prerequisite of such non-magnetic assembly is the confinement of non-magnetic building blocks in ferrofluids. As such, an external magnetic field can exert forces on magnetic particles in ferrofluids, while simultaneously exerting counteracting forces on non-magnetic components and directing their assembly (Fig. 11h).[152]

Despite the versatility of magnetic-field-guided assembly, many studies focus only on static structures formed at equilibrium. Since magnetic nanoparticles can be controlled remotely on demand, it is possible to construct small, soft robots capable of locomotion, object capture, and transportation. A classic example of the demonstration is microscopic artificial swimmers reported by Dreyfus *et al.* In their work, a flexible, magnetic filament carrying a red blood cell swam like a sperm cell under a time-changing magnetic field (Fig. 11i).[153] Following their pioneering work, other delicate motors and robots have been successfully engineered, based on magnetic components such as artificial bacterial flagella and biomimetic cilia.[154–157]

Unlike non-magnetic counterparts, magnetic nanoparticles can be readily assembled into 1D linear chains, 2D monolayer sheets, and 3D cuboids in the presence of an external magnetic field. An alternating magnetic field can maintain the superstructures out of equilibrium and regulate time-dependent and transient behaviors. While the properties of magnetic superstructures at equilibrium are fairly well understood, out-of-equilibrium magnetic superstructures pose a challenge. The intrinsic directionality of magnetic dipole interactions may render difficulty in the creation of complex reconfigurable colloidal assemblies from relatively simple components in the presence of strong interparticle magnetic interactions. For certain applications, site-specific interactions often fail to mediate self-assembly of magnetic nanoparticles into a target hierarchical structure due to difficulties in realization of site-specific surface modifications.

3.4 Lanthanide-doped nanocrystals

Lanthanide-doped nanocrystals are a special class of building blocks displaying unique optical and magnetic properties.[158] Such nanoparticles exhibit two unique luminescence mechanisms, designated photon downconversion and photon upconversion. The latter is characterized by the ability to convert two or more low-energy incident photons to a high-energy photon. This feature renders lanthanide-doped nanoparticles particularly suitable as nanoprobes for biological labeling and imaging.[159–161] Unlike quantum dots, lanthanide-doped nanoparticles do not exhibit quantum confinement because electrons in the 4f orbitals of lanthanide ions are localized due to extremely small exciton Bohr radius (< several angstroms). In addition, these lanthanide nanoparticles show a negligible interparticle coupling effect on luminescence as a result of electronic transitions in doped emitters. These two attributes allow optical properties to be accurately controlled without concerning interparticle interactions.[162]

Nanoscale forces responsible for controlling assembly of lanthanide-doped nanoparticles are almost identical to those exerted on quantum dots. This is because both lanthanide-doped nanoparticles and quantum dots are synthesized using similar strategies, including heating methods and capping ligands.[163] As a typical example, Li *et al.* used hydrophobic van der Waals interactions to assemble lanthanide nanoparticle superstructures (Fig. 12a). Using different combinations of lanthanide dopants in nanoparticle building blocks, dual-mode luminescence could be produced upon UV and near-infrared (NIR) excitation.[164,165] An extended demonstration was reported by Zhang *et al.*, who prepared upconversion luminescence-encoded superparticles by enhancing optical features of the building blocks through control over composition and doping levels in $NaYF_4$:Yb/Ln

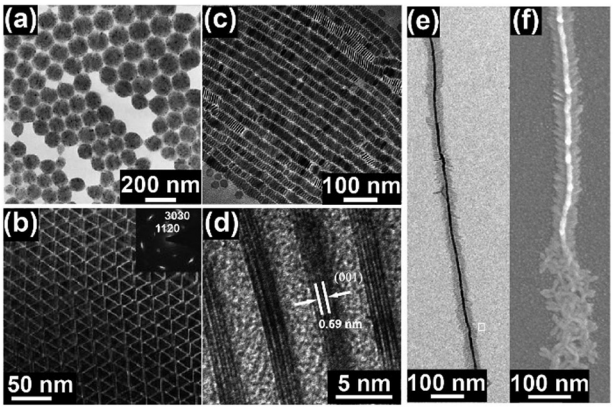

Fig. 12 (a) TEM image of colloidal spheres assembled from $NaYF_4$ nanoparticles. (b) LaF_3 nanoplate superlattices obtained *via* an edge-to-edge assembly mechanism. (c) TEM and (d) HRTEM images of La_2O_2S nanoplate superlattices. (e) TEM and (f) SEM images of 1D self-assembly of Gd_2O_3 tripodal nanoplates. (Reproduced with permission from ref. 165, 168, 169, and 172, copyright 2009, 2005, 2009, and 2013, Wiley-VCH Verlag GmbH & Co. KGaA, and American Chemical Society.)

(Ln: Er, Tm, Ho, Nd, Pr, Dy, and Sm) nanoparticles. In this study, a wide color spectrum was created for multiplex immunoassay upon 980 nm excitation.[166]

High-temperature decomposition of rare-earth precursors renders nanoparticle products with a surface layer of organic ligand such as oleylamine (OA). The presence of hydrophobic ligands on nanoparticle surfaces facilitates self-assembly *via* solvent evaporation by taking advantage of depletion and capillary attraction forces. For example, Yan's group reported the synthesis of OA-capped rare-earth oxide nanodisks and their face-to-face assembly using ethanol as antisolvent.[167] The OA capping molecules on nanocrystal surfaces extended well in hydrophobic cyclohexane solvent to prevent particle aggregation. They also demonstrated aggregation of rare-earth oxide nanodisks by increasing solvent polarity. In a follow-up work, they demonstrated edge-to-edge or face-to-face assembly of OA-caped, triangular LaF_3 nanoplates by controlling the evaporation rate of a mixed solvent. The resulting hexagonally close-packed superstructures reached several micrometers (Fig. 12b).[168] The same group also reported self-assembly of organic ligand-capped La_2O_2S and LaOCl nanoplates into various superstructures, including nanowire- and nanorod-like nanoplate arrays through exquisite control of capillary attraction forces (Fig. 12c and d).[169,170]

Anisotropic capillary attractive forces stemming from non-spherical nanoparticle building blocks can also exert orientational and positional control over ordered nanoparticle superstructures.[171–174] An intriguing study by Murray *et al.* demonstrated the assembly of tripodal Gd_2O_3 nanoplates into 1D nanofibril superstructures with two arms touching a substrate and one arm aligned parallel to the substrate (Fig. 12e and f).[172] The as-synthesized 1D superstructures could be further bundled to form ordered columnar or lamellar superstructures by tiling the nanoplate building blocks.[172] Another demonstration from the same group showed that GdF_3 nanoplates can self-assemble into long nanowires through face-to-face packing and then intertwine with shape-complementary tripodal Gd_2O_3 nanoplate arrays into bundles.[173]

For faceted nanoparticle assembly, the competition between nanoparticle shapes and interaction patchiness becomes prominent. Interaction patchiness arises from a nonhomogeneous distribution of ligand molecules on exposed facets of nanoparticles.[171,174,175] For example, $NaYF_4$ nanoparticles in the form of spheres, rods, hexagonal prisms, and plates can undergo shape-directed assembly upon gradual solvent evaporation (Fig. 13). In addition, the self-assembly process also depends on the number of nanoparticles under study. A small volume of nanorod dispersion (15 μL) facilitated superparticle synthesis with parallel *c*-axis alignment to the substrate, while a large amount of the dispersion (40 μL) led to close-packed superparticles with their long axes perpendicular to the substrate.[174] Using rhombic and irregular hexagonal rare-earth fluoride nanoplates as building blocks, Murray *et al.* demonstrated that a delicate balance between entropic and energetic effects enables long-range ordering in tiling at the liquid–air interface.[175]

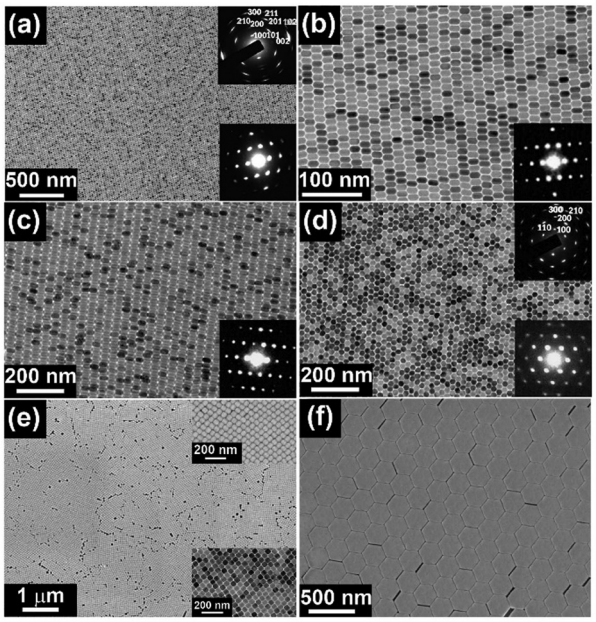

Fig. 13 (a) TEM image of a monolayer of $NaYF_4$ nanorod superlattices. The insets show corresponding wide-angle electron diffraction patterns (upper right) and small-angle electron diffraction patterns (SAED). (b and c) TEM images of a monolayer and a double-layer of nanorod superlattices. The lower right inset is the corresponding SAED pattern. (d) TEM image of a closed-packed hexagonally ordered array of vertically aligned nanorods. The insets are corresponding SAWED (upper right) and SAED patterns (lower right). (e) SEM image of a monolayer superlattice of hexagonal $NaYF_4$:Yb/Tm (22/0.2 mol%) nanoprisms. The upper right and lower right insets show high-magnification SEM and TEM images, respectively. (f) SEM image of a self-assembled superlattice of hexagonal $NaYF_4$:Yb/Er (20/2 mol%) nanoplates. (Reproduced with permission from ref. 174, copyright 2010, National Academy of Sciences, USA.)

Similar to self-assembly of magnetic nanoparticles, site-specific modification of lanthanide-doped nanoparticles for anisotropic reactivity is challenging. By taking advantage of strong interactions between negatively charged phosphates of DNA and surface lanthanide ions, lanthanide-based nanoparticle superlattices of different compositions can be prepared.[176–179] The research in this field is also motivated by the remarkable base-pairing properties of DNA as well as by its temperature-dependent reversible recognition properties. It is important to note that the molar ratio of DNA-to-lanthanide-doped nanoparticle needs to be exquisitely controlled to regulate the configuration of DNA chains on the nanoparticle surface. Random DNA attachment may induce undesirable nanoparticle aggregation due to the presence of abundant phosphates on a single DNA chain that has the ability to bind multiple lanthanide-doped nanoparticles in solution.

4. Unique properties

Nanoparticle assemblies typically display collective properties as characteristics of the whole system, but in some cases, they offer surprising discoveries and new properties. Sizes, shapes, and composition of individual particles essentially dictate

collective behavior that may not reduce to the properties of individual particles. On the other hand, coupling effects induced by proximal particle interactions may lead to unprecedented properties and functions. As a result, rational control of self-assembly is expected to yield new opportunities for multifunctional nanoparticles that will find important applications in photovoltaic and photocatalytic systems, labeling and imaging technology, and theranostic treatment.

The degree of complexity in interparticle coupling is also determined by nanoparticle uniformity in terms of size, shape, and surface ligand distribution. Control of multicomponent nanoparticle assembly is clearly a challenging task, but it promises to yield intriguing properties. In this section, we will introduce the properties offered by single-component assemblies of plasmonic, semiconducting, and magnetic nanoparticles. Following a theoretical analysis of homogenous ensembles leading to their characteristic properties, we will discuss multicomponent nanoparticle assembly using various combinations of plasmonic and semiconducting nanoparticles, as well as their associated properties.

4.1 Localized surface plasmon coupling

Surface plasmons are coherent, delocalized electron oscillations occurring on conductor surfaces. They can be resonated upon stimulation with incident light and give rise to surface plasmon resonance.[180] Of note, when the dimension of a conductor is reduced to the nanometer scale, a resonant oscillation of the electrons can be trapped and propagated along nanoconductor surfaces, giving rise to localized surface plasmons. Localized surface plasmons of individual nanoparticles show a strong dependence on particle size, morphology, composition, and refractive index of the dielectric environment.[181] For example, transformation of spherical Au nanoparticles to nanorods led to a plasmonic band splitting into two peaks, corresponding to transverse and longitudinal plasmon resonance.[182]

When individual nanoparticles are positioned within a distance five times smaller than the nanoparticle radius, the coupling between localized surface plasmons becomes distinct. Taking assembly of spherical Au nanoparticles as an example, 1D alignment of Au nanoparticles led to a new plasmonic band owing to non-equivalent resonances of longitudinal and transverse dipole polarizability.[182] Interestingly, the intensity and red-shift of the longitudinal plasmon band increased gradually with increasing length of the 1D nanoparticle chain. A similar phenomenon was observed in the shape transformation of Au nanoparticles from spherical to rod- or wire-like. In addition, coupling signals of localized surface plasmons provide detailed structural information of as-formed superparticles. For example, band broadening could be attributed to the formation of nanoparticle chains with loop, zigzag, and bifurcation features.[182] Theoretical studies based on dipole–dipole approximation verified the link of localized surface plasmons to any specific geometrical arrangement within the assemblies.

In contrast, assembly manners of anisotropic plasmonic nanoparticles have a profound impact on both longitudinal and transverse surface plasmon bands.[62] For example, as Au nanorods approached one another side-by-side, noticeable changes in both plasmon bands occurred. In contrast, end-to-end coupling of Au nanorods only led to a red-shift in the longitudinal band from 700 to 900 nm while displaying negligible changes in the transverse plasmon band.[183] In the case of end-to-end coupling, both interparticle spacing and relative orientations led to changes in the electromagnetic field and associated plasmonic properties.[184] For example, Nie and coworkers reported a 120 nm blue-shift in Au nanorod chains by increasing the interparticle gap from 6.6 to 12.9 nm.[185]

Plasmonic properties of well-separated spherical nanoparticles are well explained by Mie theory when the nanoparticle radius (R) is much smaller than the wavelength (λ) of incident light ($R/\lambda < 0.1$) (eqn (5)).[186]

$$E(\lambda) = \frac{24\pi^2 N R^3 \varepsilon_e^{3/2}}{\lambda \ln(10)} \frac{\varepsilon_i(\lambda)}{[\varepsilon_r(\lambda) + \chi\varepsilon_2]^2 + \varepsilon_i(\lambda)^2} \quad (5)$$

where N is the electron density, ε_e is the dielectric constant of the environment, ε_r and ε_i are the real and imaginary components of the dielectric function of bulk materials, respectively. χ is a factor related to the morphology of the particle. However, the emergence of surface plasmonic coupling of individual nanoparticles makes it challenging to predict surface plasmonic properties of nanoparticle ensembles. To address this issue, extended theories or methods have been developed, including plasmonic hybridization theory, Maxwell Garnett theory, the explicit particle method, and the finite-difference time-domain approach.

Here, we mainly focus on plasmonic hybridization theory for optical interpretation of plasmonic nanoparticle assemblies. In this theory, interactions of elementary plasmons of the nanoparticles are regarded in analogy to molecular orbital hybridization. Placing two spherical plasmonic nanoparticles in proximity results in two hybridized plasmonic modes: low-energy bonding plasmonic mode (energy) and high-energy antibonding plasmonic mode (Fig. 14a and b).[187] For surface plasmon coupling in two identical nanoparticles, the natural alignment between the polarization direction of incident light and the interparticle axis enables a pair of bonding–antibonding modes of σ–σ^*. Meanwhile, when the polarization direction is perpendicular to the interparticle axis, another pair of bonding–antibonding modes of π–π^* can be generated. Notably, π and π^* are formed by the out-of-phase and in-phase combination of these two plasmons, respectively, which are opposite to the longitudinal polarization associated with σ and σ^*. Modes derived from the out-of-phase combination are spectrally dark because of the cancellation effect of the equal but oppositely oriented dipoles on two identical nanoparticles. For a dimer with different sizes, all coupled plasmonic modes from either an out-of-phase combination or an in-phase combination are dipole-active as a result of incomplete cancellation of the dipoles. In the case of a composition-asymmetric dimer, for example, an Au–Ag dimer, both localized surface plasmonic bands for Au and Ag nanoparticles shifted to lower energy regions.[180] An unexpected red-shift in the surface plasmon

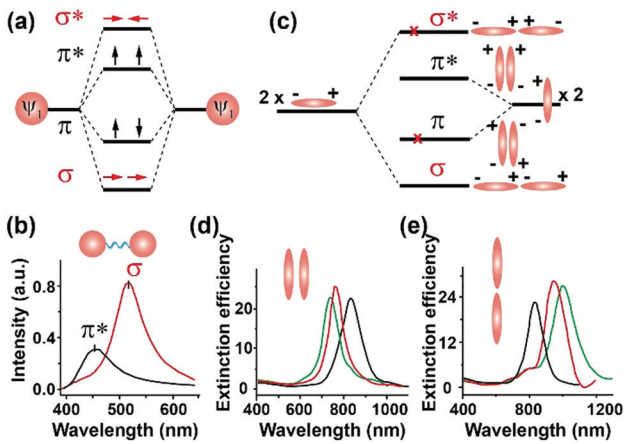

Fig. 14 (a) Plasmon hybridization model for silver nanoparticle dimers. (b) The LSPR scattering spectrum of silver nanoparticle dimers at different polarizer angles. (c) The coupled longitudinal plasmon excitation in nanorod dimers with side-by-side and end-to-end geometric arrangements and (d and e) Discrete dipole approximation-simulated extinction efficiency spectra of longitudinal plasmon excitation for gold nanorods (black: isolated nanorod, red: dimer, and green: trimer) assembled *via* a side-by-side (d) and end-to-end orientation (e). (Reproduced with permission from ref. 187 and 188, copyright 2010 and 2006, American Chemical Society.)

band of the Ag nanoparticle was ascribed to the coupling effect between the surface plasmon mode of the Ag nanoparticle and the Au interband absorption, as revealed by experimental and theoretical correlations.

The same phenomena were observed in self-assembly of Au nanorods *via* end-to-end or side-by-side attachment (Fig. 14c–e).[188] The end-to-end attachment of two Au nanorods produced a redshift in the longitudinal plasmon band (σ) relative to isolated individual nanorods. This point is analogous to a σ-bond formation from two p_z orbitals. In contrast, side-by-side attachment of two Au nanorods yielded a blue-shifted plasmonic band in the longitudinal plasmon mode, attributable to an antibonding nature of the plasmon peak in analogy to that of a π*-bond formation from $p_{x/y}$ orbitals. On a separate note, electrodynamic simulations revealed that symmetry-breaking occurs in assembling Au nanorods with dissimilar aspect ratios *via* either the side-by-side or end-to-end attachment, leading to the appearance of two components in the longitudinal plasmon band.[189]

Plasmonic hybridization theory also holds the promise of quantitatively explaining or predicting localized surface plasmonic properties of complex nanostructures, such as nanoshells, nanoeggs, nanomatryushk, and nanorices.[190–193] However, it remains challenging to accurately stimulate localized surface plasmon resonances of a long plasmonic nanoparticle chain due to complicated combinations of many plasmonic modes. Moreover, challenges in precise optical characterization of the assemblies at the nanometer level impose additional limitations in experimental validation of theoretical calculations.

4.2 Plasmonic circular dichroism

Circular dichroism (CD) is a state-of-the-art technique for probing the difference of molecules in the extinction of right and left circularly polarized light.[194] There are two main strategies used for preparation of chiral plasmonic nanoparticle ensembles showing a CD effect. One involves use of chiral organic ligands to modify nanoparticle building blocks.[195,196] The other involves placement of plasmonic nanoparticles in a secondary architecture bearing a non-superposable mirror image.[197,198] In the latter case, interparticle plasmonic dipole–dipole interactions can generate a surface-plasmon CD in the vicinity of localized surface plasmon bands.

In principle, chiral ensembles can be classified as chiral nanoparticle molecules or chiral nanoparticle polymers. For example, Mastroianni and coworkers placed different-sized Au nanoparticles on the tip of a pyramidal nanostructure and further synthesized chiral Au tetramers with the help of double-stranded DNA sequences.[69] In their design, two enantiomers (*R* and *S* configuration) were produced by precisely controlling the relative spatial locations of the monomers. However, chiral tetramer purification from the mixture was challenging, making optical studies of the diastereomer difficult. Similarly, other complementary nanoscale forces between biomolecules, including hydrogen-bonding and van der Waals force, could also be utilized to construct chiral nanoparticle assemblies.[199–201] For example, DNA-based self-assembly allows the preparation of 1D chiral plasmonic nanostructures with a tunable optical response.[73] The colloidal solution of assemblies exhibits well-defined CD and optical rotatory dispersion effects in the visible region, in good agreement with theoretical calculations based on classical electrodynamics (Fig. 15a–d). CD signals of synthesized plasmonic polymers were much stronger than those of individual plasmonic monomers due to plasmon coupling after nanoparticle alignment. Left-handed or right-handed plasmonic Au nanoparticles could be obtained in high purity by rational design of DNA scaffolds, laying the foundation for unraveling optical difference in these diastereomers.

4.3 Plasmon–exciton coupling

For binary component assemblies comprising plasmonic nanoparticles and quantum dots with homogeneous distributions, interactions between the two components within a few nanometers strongly impact overall properties of the ensembles. For example, plasmon–excitation coupling has a significant influence on optical absorption. When a quantum dot is placed proximal to a plasmonic nanoparticle, light can be confined to the gap between the two nanoparticles. This light confinement leads to enhanced electromagnetic fields, thereby broadening the absorption cross-section of the quantum dot. Indeed, surface plasmons of noble metal nanoparticles have proven effective in enhancing absorption and luminescence in semiconducting nanocrystals.[202,203] Exciton dynamics of quantum dots are influenced by plasmon–exciton coupling, as evidenced by an enhanced radiative rate along with emission quenching of the quantum dots. In addition, emissions of quantum dots can be transferred to proximal plasmonic nanoparticles, accompanied by a decrease in photoluminescence intensity. Taken together, the emission intensity of binary assemblies is

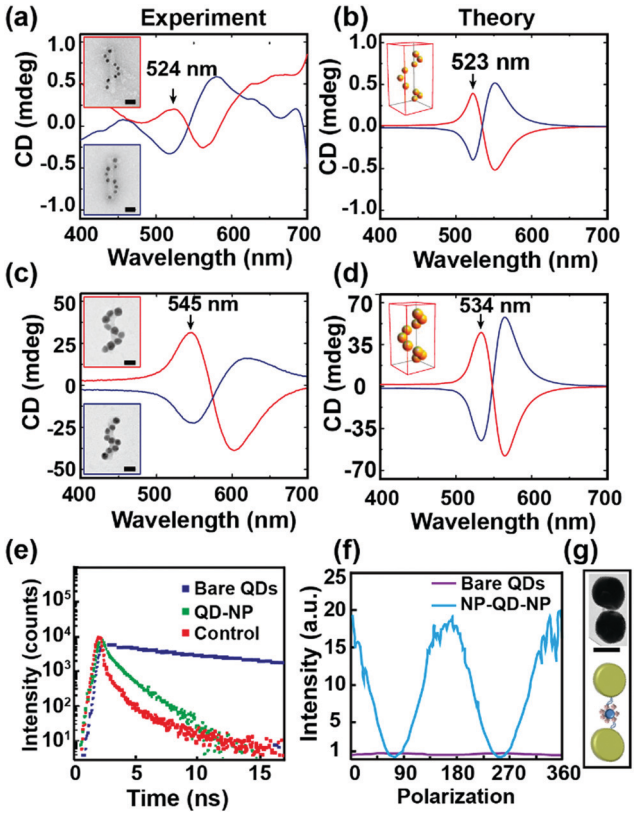

Fig. 15 Experimental (a and c) and theoretical (b and d) CD spectra of left-handed (red line) and right-handed (blue line) helices formed by nine Au nanocrystals. (e) Decay curves of bare quantum dots (blue), quantum dot-Au nanoparticle hybrids (green), and controls (red). (f) Emission intensity of a single nanoparticle–QD–nanoparticle structure (blue line) and individual QDs (purple line) as a function of the polarization angle. (g) TEM images (upper) and schematic model (bottom) of Au nanoparticle–quantum dot hybrid. (Reproduced with permission from ref. 73 and 204, copyright 2012 and 2012, Nature Publishing Group, and American Chemical Society.)

the sum of plasmon-enhanced emission and nonradiative energy transfer between the quantum dot and the plasmonic nanoparticle.

A set of parameters involving plasmonic nanoparticles and quantum dots can affect plasmon–exciton coupling. In general, a good spectral overlap between the excitation of quantum dots and the plasmonic band of metal nanoparticles may lead to strong plasmon–exciton coupling. Furthermore, the relative location of the pair and the nature of material composition are also essential to determine the plasmon–exciton coupling effect. A case in point was the study of a quantum emitter after being positioned in a plasmonic gap.[204] The researchers observed a nearly 20-fold enhancement in fluorescence intensity and a three-order-of-magnitude reduction in the excited-state lifetime (Fig. 15e–g). In a case study of binary assembly of CdSe quantum dots and Au nanocrystals, Shevchenko and coworkers reported that fluorescence quenching typically occurs when the plasmonic gap is comparable to the length of stabilizer molecules (1.5 nm).[205] Silica, polymers, and DNA molecules can be utilized as spacers to tune the size of the plasmon gap for optimal plasmon–exciton coupling. In 2007, Lee *et al.* reported that the plasmon–exciton coupling based on an Au-modified CdTe nanowire could lead to a blue-shift of the emission color.[206]

4.4 Exciton migration

Exciton migration in luminescent nanoparticle ensembles is an intriguing phenomenon and characterized by a set of changes in optical properties, including a redshift in emission band, fluorescence quenching, and shortened emission lifetime. Excitons can migrate distances up to several micrometers. Förster resonant energy transfer (FRET) is a powerful technique for studying energy transfer between nanoparticles, with a high spatial resolution typically in the range of 1–10 nm and without the need for the overlapped wavefunction. A combination of tuning interparticle distance and engineering the bandgap of nanoparticle ensembles in a multilayer film presents an effective way to regulate exciton migration and fabricate 2D optoelectronic devices.[207,208]

Using single-component, monodisperse quantum dots as building blocks, a red-shifted emission profile in the solid-state, relative to the solution phase, was achieved. This shift is likely induced by a decrease in the separation distance between the quantum dots after solvent evaporation, improving interparticle energy transfer.[209,210] Note that the concentration of quantum dot building blocks can also affect optical emission upon nanoparticle assembly because a high concentration allows superlattices to be formed with less disordering. In addition to exciton migration in single-crystalline superlattices, considerable attention was paid to interparticle energy transfer within polycrystalline fluorescent dendrites comprising CdSe/ZnS quantum dots or rods.[211,212] In these two cases, energy transfer from the periphery to the dendrite core was elucidated by steady-state and time-resolved photoluminescence spectroscopy. The high quantum yield of quantum dots significantly affects interparticle coupling and thereby the Förster radius, leading to directional energy transfer with high efficiency.[213]

Alternatively, nanoparticle assemblies can be prepared with different-sized quantum dots *via* layer-by-layer assembly. Upon assembly, fluorescence quenching of small nanoparticles is typically accompanied by a concomitant emission increase in large nanoparticles. Such an optical scenario is attributed to dipole coupling between proximal quantum dots. In pioneering work, Kagan and coworkers reported long-range electronic exciton transfer from small CdSe quantum dots (3.85 nm) to their larger counterparts (6.2 nm) in close-packed solids.[214] In their study, both interparticle distance and spectral overlap between donor emission and acceptor absorption dictated energy transfer efficiencies. When poor spectral overlap occurred between PbS nanocrystals of two different sizes, exciton transfer was confirmed to be relatively weak by steady-state and time-resolved photoluminescence studies.[209] Guo *et al.* reported somewhat similar results when investigating 2D film made of CdSe@ZnS core–shell quantum dots of different size.[215]

Directional exciton migration within multiple-layer ensembles has been achieved by rational alignment of the energy bandgap of quantum dots in different layers. A bilayer of CdSe@ZnS quantum dots of different size was first exploited by Klimov and coworkers as energy-gradient layered structures to demonstrate layer-to-layer energy transfer with a 750 ps FRET time.[216] The interlayer FRET time was further accelerated to 50 ps by Franzl *et al.* in a two-layered system comprising two sets of CdTe nanocrystals (2.8 and 3.4 nm).[217] The short-distance energy transfer led to efficiencies as high as 80%. In an elaborate multilayered system, cascaded energy transfer was achieved *via* layer-by-layer assembly of a series of CdTe nanocrystals (1.7, 2.5, 3.2, and 3.5 nm).[218] As expected, directional excitation energy transfer drastically enhanced the red emission in the intermediate layer, while completely suppressing orange, yellow, and green emissions in the outer layers (Fig. 16). It should be pointed out that cascading energy transfer along a decreasing bandgap gradient in multi-layered assemblies closely resembles light-harvesting in natural complexes, holding great promise for applications in electronics and optoelectronics.[219]

4.5 Interparticle dipolar interaction

Permanent magnets are characterized by a hysteresis loop that defines how magnetization changes as a function of an applied field.[220–224] As with electric dipoles, magnetic dipoles of magnetic materials tend to align with an applied external field. If the axis of magnetic dipoles and the external field direction match, the value of the magnetization reaches saturation magnetization (M_s) where potential energy is at a minimum. Upon removal of the applied external field, the remaining induction in the magnetic material is called remanence magnetization (M_r). The magnitude of the external field applied in the reverse direction to bring the magnetization of the sample back to zero is called the coercive field.

Assemblies of magnetic nanoparticles will impart new collective properties due to interparticle dipole interactions. Anomalous magnetic properties can be discovered by measuring magnetization as a function of an external magnetic field or temperature. For example, in the study of magnetic behaviors of cobalt nanoparticle assemblies, their geometrical arrangement was found to have a significant impact on magnetic properties.[225,226] The coherent anisotropy in disordered assemblies led to a greater energy barrier relative to ordered superstructures, resulting in a broader zero-field-cooled (ZFC) peak (Fig. 17a). In addition, a high coercive field and a slow rate of saturation were also observed in self-assembled, magnetic nanoparticle superstructures with a high-level structural ordering (Fig. 17b).[227–229]

The shape and packing density of magnetic nanoparticle assemblies also influence the magnetic properties of the resultant superparticles. For example, magnetic γ-Fe_2O_3 nanocrystals tend to self-assemble into long wires or homogeneous films in the presence of surfactants. When applying field direction along the long axis (x-direction) of the wire, the remanent magnetization was increased compared to that obtained along the short axis (y-direction).[227] In contrast, no changes were recorded in the magnetization curve for homogeneous films (Fig. 17c). This phenomenon suggests that 1D magnetic wires resemble single, elongated particles and their cooperative

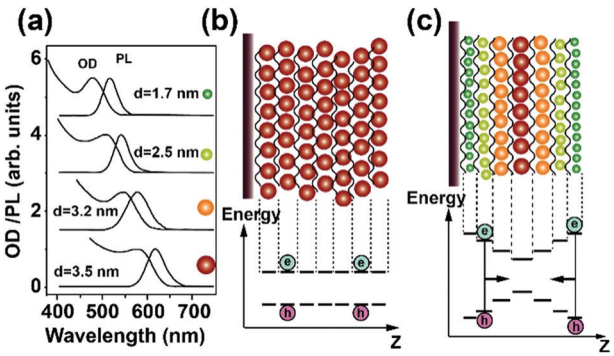

Fig. 16 (a) Absorbance and photoluminescence spectra of four different sized CdTe nanocrystals used for the preparation of a layer-by-layer assembled film. (b) Schematic illustration of the resonant energy transfer within the device consisting of seven layers of 3.5 nm CdTe nanocrystals (upper) and energetic positions of the highest occupied nanocrystals orbital (HONCO) and the lowest unoccupied nanocrystal orbital (LUNCO)in the resulting nanoparticle film (below). (c) The cascaded energy transfer within a layer-by-layer assembled film using quantum dots of different size (upper) and the corresponding energy levels within the resulting nanoparticle film. (Reproduced with permission from ref. 218, copyright 2004, American Chemical Society.)

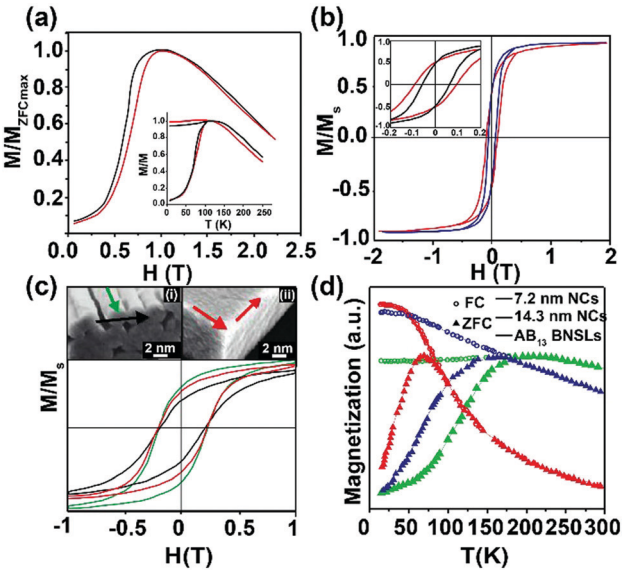

Fig. 17 (a) ZFC curves of amorphous aggregates (red) and supercrystals (black). (b) *M versus H* curves of disordered (black line) and ordered (red line) 3D assemblies. Inset: Enlargement of the low-field region. (c) SEM images of shaped γ-Fe_2O_3 nanocrystals coated with (i) citrate ligand to form a tubular morphology and (ii) with decanoic acid to form a thin film. Magnetization curves at 3 K of the tubes, recorded with different alignments. (d) ZFC/FC curves recorded for 14.3 nm Fe_3O_4 nanoparticles (olive), 7.2 nm Fe_3O_4 nanoparticles (red), and the resulting film of AB_{13}-type nanoparticle superlattice (blue). (Reproduced with permission from ref. 227 and 230, copyright 2007 and 2010, American Chemical Society.)

response is more sensitive to the magnetic field than that of discrete nanoparticles. In 2010, Murray and coworkers reported magnetization measurements of a binary AB_{13} superlattice comprising two types of Fe_3O_4 nanoparticles of different size as a function of temperature (Fig. 17d). The binary superlattice exhibited a single-phase-like transition, which is different from phase-separated, stoichiometric nanoparticle mixtures.[230]

Current research on optical, electronic and magnetic characterizations of nanoparticle superlattices lays the foundation toward a better understanding of structure–property correlations. This understanding will help tackle the self-assembly of nanoparticles into superstructures where complexity emerges from the interplay of particle interactions and the competition of force due to solvent interactions. As characterizations of nanoparticle superlattices are typically performed in ensemble forms, reliable data need to be acquired from highly uniform samples. This is because that subtle variations in defects or impurities in superlattices can lead to substantial changes in their properties.[231] In fact, this is somewhat akin to doping of foreign atoms, such as P and As, into atomic lattices of host materials, such as Si. To determine the properties of isolated individual superparticles, single-particle characterization tools or techniques need to be developed.

5. Emerging applications

Nanoparticle assemblies displaying unusual properties are likely to find important applications in biosensing, drug delivery, therapeutics, energy conversion devices, and nanoelectronics. Apart from intrinsic properties possessed by individual nanoparticle building blocks, new properties acquired during assembly can be utilized to sense or probe a variety of analytes, such as metal ions and biomolecules.

5.1 Biological sensing

Mirkin and colleagues pioneered the application of plasmonic nanoparticle assembly for DNA sequencing.[63,232] This technology is based on hybridization of DNA strands tethered on the surface of Au nanoparticles with target oligonucleotides. DNA sequence hybridization induces a colorimetric change in the colloidal solution, which is readily detectable by the naked eye. Since its discovery in 1996, this colorimetric method has been widely used for biomolecular detection, environmental pollutant screening, and understanding of biological processes, including DNA hybridization, bending in transcription complexes and cleavage at moderate temperatures.[233] In addition to utilization of aggregation-induced color changes, variations in interparticle distance through precise design of surface chemistry can create optical sensors for analytical applications. One outstanding example was reported by Alivisatos and co-workers, who studied kinetics of DNA hybridization using a ''molecular ruler'' based on plasmon coupling of gold and silver nanoparticles.[234] When biotin-modified, single-stranded DNA(ssDNA)-functionalized Au nanoparticles were added to a solution of streptavidin-coated Au or Ag nanocrystals, scattered colors changed from blue to blue-green, or green to orange, indicative of Au–Ag or Au–Au dimer formation (Fig. 18a and b). Upon addition of complementary DNA strands to the Au–Au dimer solution, a blue-shift of the light-scattering spectrum was observed (Fig. 18c). The authors ascribed this phenomenon to double-stranded DNA (dsDNA) formation. dsDNA has much stiffer framework than ssDNA, driving dimer dissociation to form separated Au nanoparticles.[234]

As already described in previous sections, plasmonic gaps or hotspots can be engineered by controlling interparticle distances between plasmonic nanoparticles. Formation of plasmonic hotspots enables five to eight orders of magnitude of signal enhancement in surface-enhanced Raman scattering (SERS) as a result of large electromagnetic field enhancement.[235–237] The size match between the plasmonic gap and cellular organelle and the ease of achieving strong scattering intensity with SERS make it possible to perform real-time investigation of the organelle environment in living cells. A proof-of-concept work was demonstrated by Kotov and co-workers,[68] who made three types of assemblies using Au nanoparticles and nanorods by selective modification of nanorods with DNA oligomers. After incubation of Au assemblies with HeLa cells at 37 °C under 5% CO_2 for 12 h, they observed strong SERS signals from intracellular, unsaturated lipids in the mitochondria.[68]

Photoluminescence changes of assemblies of semiconductor and metal nanoparticles are also applicable to molecular sensing through exciton–plasmon interactions. For instance, assemblies of amine-terminated Au nanorods and carboxyl-terminated CdTe@CdS quantum dots showed a high FRET efficiency and induced emission quenching of the quantum dots.[238] Upon addition of 2,4,6-trinitrotoluene (TNT) molecules, the preformed assemblies disassociated due to TNT complexation by quantum dots, giving rise to a switchable luminescence response (Fig. 18d and e).[238] In another example, Kotov and coworkers designed superstructures comprising CdTe nanowires and Au nanoparticles connected by polyethylene glycol (Fig. 19a–c).[206] The altered distance between the CdTe nanowire–Au nanoparticle couple, enabled by modulating the interaction between antibodies (aB) incorporated in the polyethylene glycol molecular backbone and added antigens (aG), imparted a noticeable emission wavelength shift due to exciton diffusion in CdTe nanowires.

Since 2010, CD plasmonics has emerged as a new detection method for probing chiral bioactive molecules and optical materials.[201] For example, in 2012 Tang's group demonstrated reversible changes in plasmonic CD responses by taking advantage of temperature-dependent assembly and disassembly of Au nanorods with DNA strands (Fig. 19d–g).[239] After Au nanorod assembly, changes in the intensity and line shape of plasmonic CD signals are more distinct than in UV-vis absorption spectra. Therefore, this CD-based analytical platform offered an ultra-sensitive capacity for DNA detection with a detection limit of 75 nM.[61,239–241]

5.2 Drug delivery and therapy

In nanomedicine, site-specific delivery and controlled release of drugs by nanocarriers remain a major challenge as drug efficacy

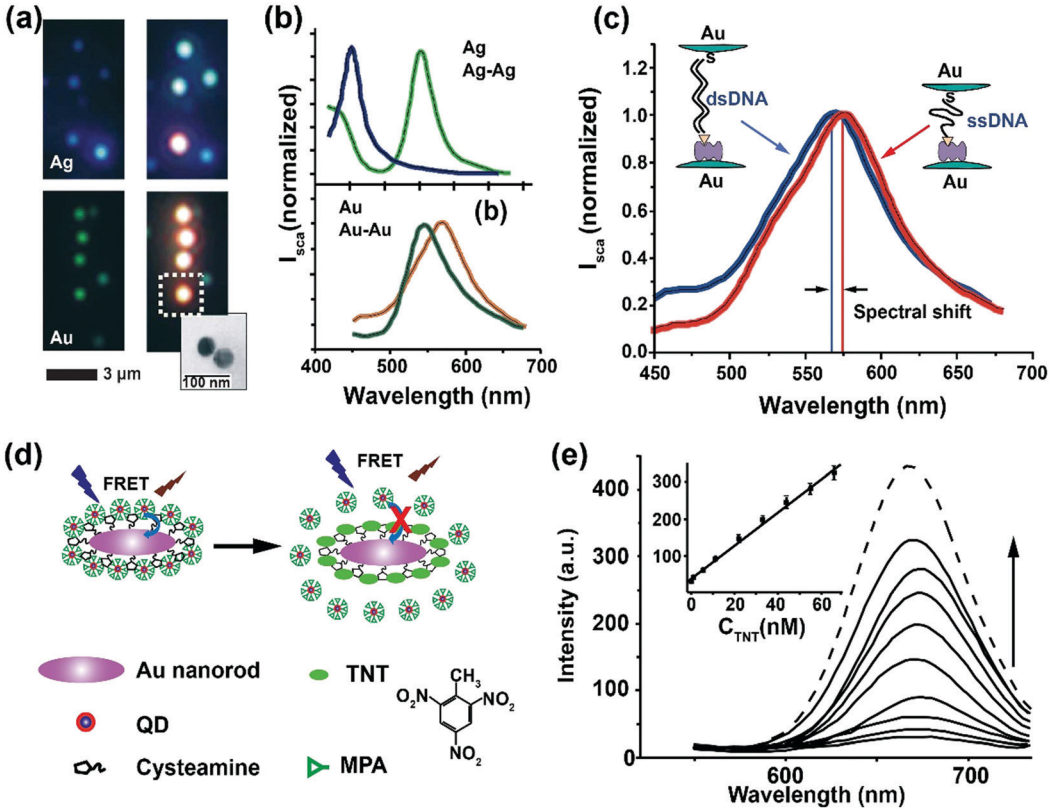

Fig. 18 Color effect based on an assembly of DNA-functionalized gold and silver nanoparticles: (a) the color changed from blue for single silver particles (upper left) to blue-green for particle pairs (upper right). Single gold particles appear green (bottom left) and gold particle pairs exhibited orange (bottom right). Inset: Representative transmission electron microscopy image of a particle pair. (b) Representative scattering spectra of single particles and particle pairs for silver (top) and gold (bottom). (c) The spectral shift between a gold particle pair connected with ssDNA (red) and dsDNA (blue). (d) Schematic illustration of the FRET-based operating principle for Au nanorod-quantum dot assembly. (e) Evolution of emission spectra of Au nanorod-quantum dot assemblies with increasing TNT analyte. (Reproduced with permission from ref. 234 and 238, copyright 2005 and 2011, Nature Publishing Group and American Chemical Society.)

is usually determined by non-specific cell and tissue biodistributions of the loaded drugs. Released drugs are rapidly metabolized or excreted from the body. Self-assembled nanostructures are attractive as promising theranostic tools for drug delivery and therapy because they are sensitive to external stimuli. A well-documented example was reported by Duan *et al.*, who assembled plasmonic vesicles from Au nanoparticles and amphiphilic polymers for cancer-targeted drug delivery.[242] Their study suggests that an acidic intracellular environment can lead to a hydrophobic-to-hydrophilic transition in hydrophobic brushes, enabling triggered intracellular drug release.

Implementation of nanoparticles for targeted delivery and controlled release of therapeutic agents in endocytic organelles could be achieved through assembly and disassembly of plasmonic nanoparticles with a hollow cavity under different pH conditions.[242] In addition, due to a strong interparticle plasmonic coupling, self-assembled plasmonic vesicles showed different plasmonic properties and greatly enhanced SERS intensity compared to single gold nanoparticles. Thus, disassembly of vesicles in endocytic organelles led to dramatic changes in scattering properties and SERS signals, serving as independent optical and spectroscopic feedback for cargo release from the vesicles.

Photosensitive entities have added benefits to nanoparticle assemblies for clinical applications. NIR-responsive systems have previously shown promise of reduced damage to tissues and improved tissue penetration in drug delivery and therapy.[243–245] One notable strategy is to add NIR-absorbing plasmonic nanoparticles to assembled nanocarriers. Upon NIR irradiation, the light can be converted into heat. This *in situ* heat generation could trigger the release of chemotherapeutic molecules from the nanocarriers. For instance, when Au nanorods loaded with doxorubicin were irradiated by NIR light, the light-to-heat transduction elevated the temperature in the vicinity of the Au nanorods and induced DNA dehybridization on nanoparticle surfaces, triggering the release of doxorubicin molecules.[246,247]

Nie and co-workers applied a multifunctional theranostic platform based on photosensitizer-loaded plasmonic vesicles for *in vivo* cancer imaging and treatment.[248] The vesicular architecture composed of a monolayer of Au nanoparticle assemblies showed strong absorption in the range of 650 to 800 nm. By encapsulating photosensitizers, this platform showed a dual imaging and therapeutic capability.[248] In 2013, this strategy was used by the same group to prepare biodegradable plasmonic vesicles for photoacoustic imaging and photothermal therapy.[249]

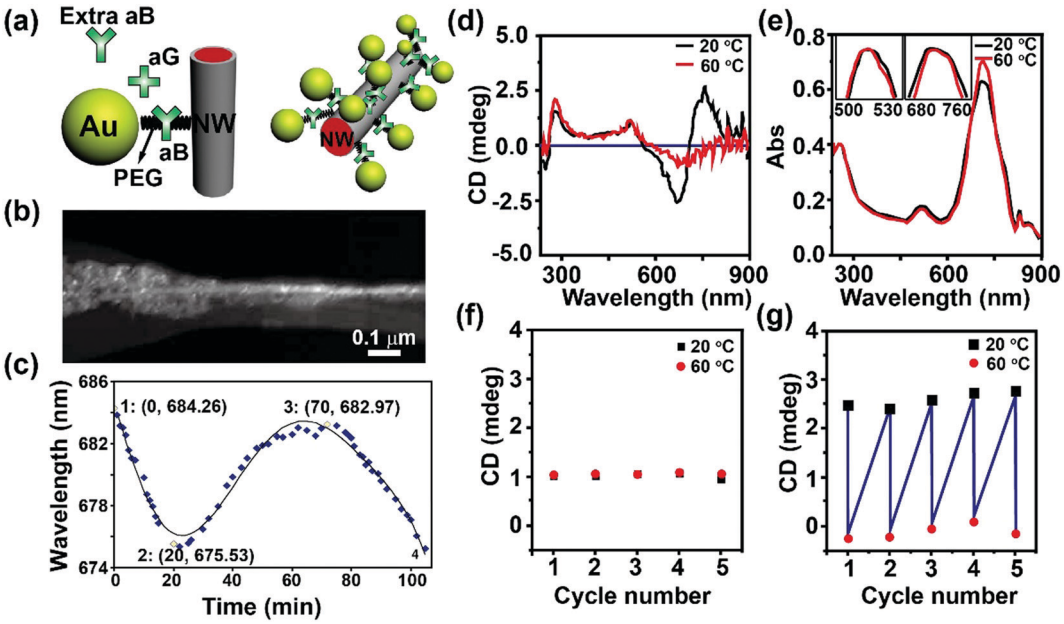

Fig. 19 (a) Schematic illustration of aG–aB interaction in molecular spring assemblies comprising Au nanoparticles and CdTe nanowires. (b) TEM imaging of as-formed Au–PEG–aB–PEG–nanowire structures. (c) The reversible emission wavelength shift of the peak: 1, attachment of a nanoparticle to a nanowire; 2, after adding 20 μL streptavidin; 3, after adding free aB to the media; 4, after adding 20 μL anti-streptavidin. (d) The reversible plasmonic CD and (e) corresponding UV-vis absorption spectra of DNA-modified Au nanorods at 20 °C (black line) and 60 °C (red line). (f) CD intensity at 512 and 750 nm, (g) CD intensity as a function of cycle numbers at 20 °C (black dots) and 60 °C (red dots). (Reproduced with permission from ref. 206 and 239, copyright 2007 and 2012, Nature Publishing Group and American Chemical Society.)

After completion of their therapeutic function, biodegradable vesicles disintegrated into smaller discrete units and underwent rapid clearance (Fig. 20).

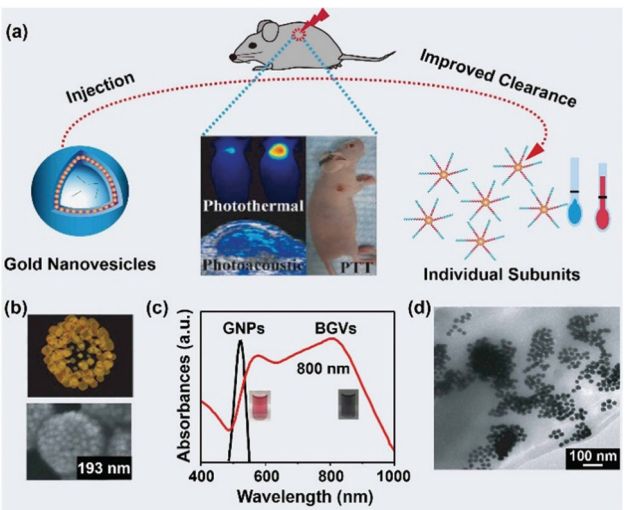

Fig. 20 (a) Schematic representation of multifunctional plasmonic vesicles for *in vivo* photoacoustic imaging and photothermal therapy with improved clearance after the dissociation of the assemblies. (b) 3D electron-density mapping of a broken biodegradable gold vesicle (BGVs, upper) and TEM image of individual vesicles (bottom) with a size of 193 nm. (c) UV/Vis/NIR spectra of gold nanoparticles and BGVs. (d) TEM image of the disassembled gold subunits from BGVs after treatment at 100 °C for 10 min. (Reproduced with permission from ref. 249, copyright 2013, Wiley-VCH Verlag GmbH & Co. KGaA.)

Such assemblies, showing potential to use NIR light in theranostic applications, are based on utilization of lanthanide-doped upconversion nanoparticles as light converters. These nanoparticles hold promise to combine two or more incident photons into one UV or visible photon.[250–252] An example has been demonstrated by Lu *et al.*, who reported target recognition *via* the interaction between DNA-modified upconversion nanoparticles and Au nanoparticles based on a self-assembly strategy.[177] Furthermore, DNA-modified upconversion nanoparticles can be used for DNA delivery and targeted imaging of cancer cells.

In addition, recent studies have attempted to create efficient drug delivery systems by combining magnetic nanoparticles with an external magnetic field. Such stimulus-responsive drug release systems could provide site-specific drug targeting and retention with a magnetic field gradient by concentrating the magnetic nanocarriers at target cells or tissues.[253–256] As an added benefit, self-assembled magnetic superstructures have shown improved magnetic responsiveness compared to individual nanoparticles, enabling ease of regulation of the nanocarriers by an external magnetic force. For example, assembly of magnetic nanoparticles and anticancer drugs in amphiphilic polymers has been reported by Huh, Haam, and co-workers.[255] Therapeutic antibody-decorated superstructures showed ultrasensitive targeted detection by magnetic resonance imaging (MRI) in *in vitro* and *in vivo* models (Fig. 21a). Moreover, the composite superstructures indicated excellent synergistic effects for inhibition of tumor growth.[255] In a parallel investigation, magnetothermally responsive doxorubicin-encapsulated supramolecular

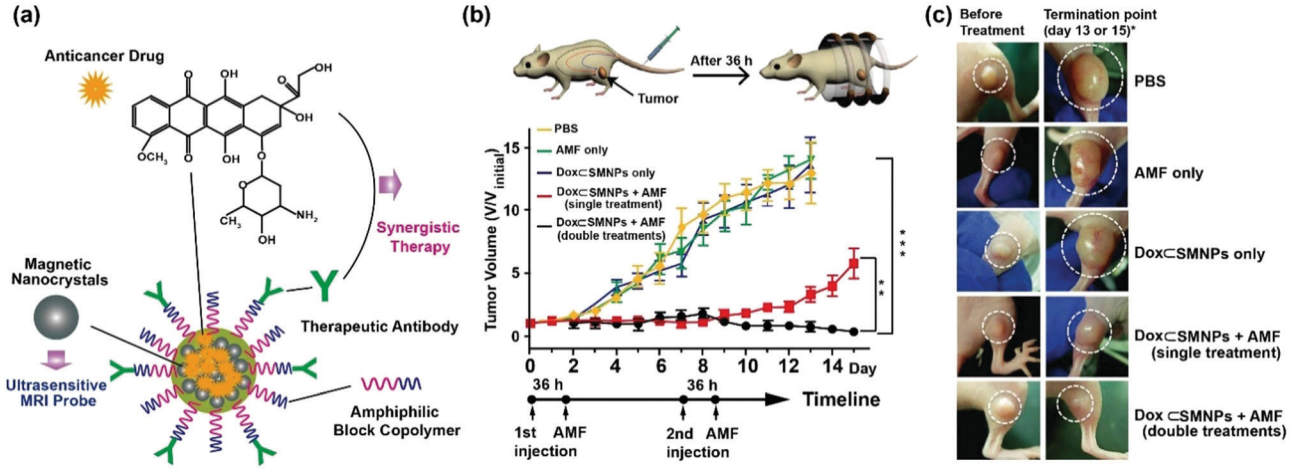

Fig. 21 (a) Schematic representation for fabrication of multifunctional magnetic nanohybrids encapsulated with doxorubicin. (b) Application of the as-prepared Dox⊂SMNPs in tumor therapy in a mouse model. (c) Tumor images without and with the application of Dox⊂SMNPs under different conditions. (Reproduced with permission from ref. 255 and 257, copyright 2007 and 2013, Wiley-VCH Verlag GmbH & Co. KGaA.)

magnetic nanoparticles (Dox⊂SMNPs) have been designed by Cheon, Tseng, and coworkers as a unique on-demand drug delivery/release system.[257] These self-assembled magnetic assemblies consisting of $Zn_{0.4}Fe_{2.6}O_4$ superparamagnetic nanoparticle, polymer, and anti-cancer drugs, could be preferentially accumulated at the site of a tumor. More importantly, these magnetic nanoparticles could convert the radiofrequency of an external alternating magnetic field (AMF) into heat, allowing on-demand stimulus-responsive drug release from the supramolecules (Fig. 21b and c).

5.3 Energy conversion devices

The advent of large-scale structures through nanoparticle assembly paves the way toward device fabrication for advanced energy conversion. Currently, superlattices for energy conversion applications are based on controlled emulsion assembly of preformed nanoparticles into 3D superlattices, followed by annealing at high temperatures.[258] The annealing treatment transforms surface ligands to conductive carbon coatings on nanoparticle surfaces, improving electron transport efficiency and suppressing nanoparticle aggregation.[259–261]

In 2015, Zheng *et al.* reported the synthesis of monodisperse oleic acid-protected CoMnO nanoparticles and performed micellization of the nanoparticles in hexane in the presence of squalane (1 wt%). Subsequent annealing at 550 °C under an argon atmosphere in the presence of urea for 2 h led to the formation of 3D interconnected CoMnO@N-doped carbon nanoparticle superlattices.[262] The resulting superlattices showed high electrocatalytic activity toward water splitting in KOH (1.0 M), as evidenced by an onset potential at 1.46 V (*vs.* RHE) for the oxygen evolution reaction and by an overpotential of 71 mV at 20 mA cm^{-2} for the hydrogen evolution reaction. Similar strategies have been used by Yang and Dong *et al.* to develop Fe@carbon superparticles as electrocatalysts for denitrification using oleic acid-protected Fe_3O_4 nanoparticles as the building blocks. With such electrocatalysts, the removal capacity was estimated to be as high as 1816 mg N g^{-1} Fe with a nitrogen selectivity up to 98% in the presence of 100 mg L^{-1} nitrate.[263] On a separate note, controllable etching of metal oxide nanoparticles within the treated superlattices allows developments of highly ordered single-atom electrocatalysts for oxygen reduction reaction and mesoporous few-layer graphene frameworks for lithium-ion batteries.[264,265]

For energy conversion, the performance of nanoparticle superlattice-derived catalysts can be further enhanced by geometric arrangement of the nanoparticles. Close-packed nanoparticles can block mass transport and hinder molecular interactions at catalytic sites. To address this issue, the Dong group reported an interesting method toward fabrication of freestanding, carbon-coated hollow Mn_3O_4 nanoparticle superlattices.[266] They first assembled a monolayer of oleic acid-capped MnO nanoparticles into porous anodized aluminum oxide (AAO) templates. The MnO nanoparticle-functionalized AAO template was subjected to controlled annealing and etching in KOH (6.0 M), resulting in hollow Mn_3O_4 tubular monolayer superlattices (h-Mn_3O_4-TMSLs) (Fig. 22a–e). Their high performance in oxygen reduction was supported by the onset potential at ~0.91 V (*vs.* RHE) and the 5.7 mA cm^{-2} diffusion-limiting current density in the rotating disk electrode polarization curve (Fig. 22f and g). Furthermore, the electrocatalysts showed an average electron transfer number of 3.91, which is higher than that of the controls, including MnO-TMSLs and solid Mn_3O_4-TMSLs counterparts (s-Mn_3O_4-TMSLs) (Fig. 22h). In addition to high catalytic activity, h-Mn_3O_4-TMSLs displayed better long-term catalytic stability than state-of-the-art Pt/C catalysts under identical conditions (Fig. 22i).

Alternatively, the performance of nanoparticle superlattices for energy conversion applications can be improved by controlling the composition of constituting nanoparticle building blocks. Recently, Dong and coworkers reported that binary $CoFe_2O_4$–Fe_3O_4 nanocrystal superparticles with a carbon layer show better lithium storage than their single-component

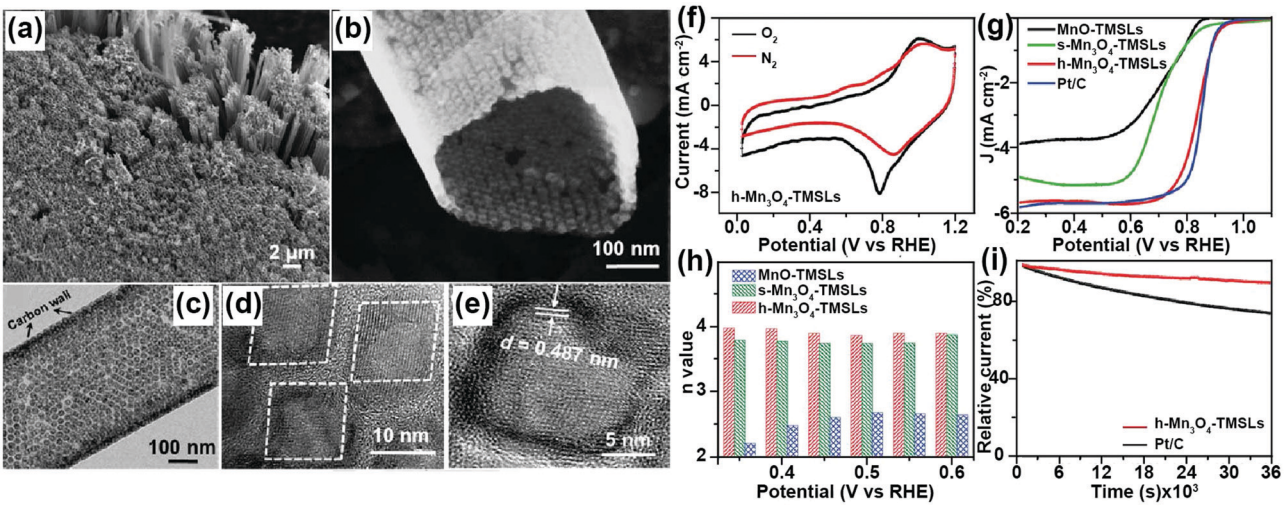

Fig. 22 (a and b) Low- and high-magnification SEM images of as-prepared h-Mn_3O_4-TMSLs. (c and d) Low- and high-magnification TEM images of h-Mn_3O_4-TMSLs. (e) HRTEM image of a single hollow Mn_3O_4 nanocrystal. (f) Cyclic voltammogram curves of h-Mn_3O_4-TMSLs in N_2- and O_2-saturated alkaline solution (0.1 M KOH), respectively. (g) Polarization curve comparison of MnO-TMSLs, s-Mn_3O_4-TMSLs, h-Mn_3O_4-TMSLs, and Pt/C at a rotation speed of 1600 rpm. (h) Potential-dependent electron transfer number recorded for MnO-TMSLs, s-Mn_3O_4-TMSLs, and h-Mn_3O_4-TMSLs. (i) Chronoamperometric measurements of h-Mn_3O_4-TMSLs and Pt/C. (Reproduced with permission from ref. 266, copyright 2017, American Chemical Society.)

superlattices.[267] Also, the binary nanoparticle superlattices also showed better lithium storage than those physically mixed binary samples. After 500 catalytic cycles, the binary superlattices retained a high capacity of ~800 mA h g^{-1} relative to 630 mA h g^{-1} for the physically mixed samples. Mechanistic studies suggest that the improved performance is attributed to more open space accessible in the carbon-coated binary nanoparticle superlattices than that of their single-component counterparts. The open space not only enables better mass transport but also alleviates volumetric changes in superlattices, maintaining the structural integrity of the anode materials during repeated lithiation and delithiation.

5.4 Other applications

Besides the above-mentioned applications, effects of nanoparticle assembly can be harnessed to develop other technological applications. Taking magnetic nanoparticles as an example, magnetoresistive devices could be fabricated by assembling a mixture of Fe_3O_4 and FePt nanoparticles into 2D membranes. The magnitude of magnetoresistance showed a dependence on the stoichiometry of binary assemblies. AlB_2-type membranes exhibited higher magnetoresistance values than icosahedral-AB_{13}-type equivalents.[128] In a separate study, multifunctional assemblies of magnetic and metal nanoparticles were used for protein separation.[268] With the help of Au nanoparticles, proteins could be easily adsorbed to the metal part of Au-Fe_3O_4 hybrids. With the help of an external magnetic field, the hybrids with adsorbed proteins were easily separated from the fluid phase.

6. Conclusion and perspective

In this review, we attempted to highlight recent advances in inorganic nanoparticle assembly. Assemblies described in this review exhibit variations in structures, depending on the nature of nanoparticle building blocks and different strategies applied. There is a large resemblance between nanoparticle self-assembly and atom- or molecule-level reactions. Nanoscale forces are the most important parameters determining the direction, strength, and length of nanoparticle bonds within the assemblies. Nanoparticle bonding is not only affected by intrinsic attributes of nanoparticle monomers, but also by experimental conditions, including concentration, temperature, and solvent polarity. These provide versatile tools to control the self-assembly process, while rendering additional challenges to reproduce experimental results.

Compared to the controllability of reactions at the atomic or molecular level, research in nanoparticle self-assembly is still at an early stage. One of the most challenging tasks is the lack of a general and effective method to equip nanoparticle monomers with directional reactivity. If this goal can be achieved, additional controllability may be acquired by controlling cross-sections of nanoparticle reactants based on collision theory. An alternative method is learning from biosystems capable of generating complex molecular assemblies from a collection of individual molecules.

With nanoparticle reactants in reserve, understanding the thermodynamic and kinetic factors that dictate self-assembly behavior provides insights into the development of superstructures with desirable macroscale properties. As complementary tools, multiscale computational simulation comprising different theoretical characters may reveal quantitative correlations between geometric structures and physical/chemical properties of nanoassemblies under study. Specifically, when combining density functional theory and molecular dynamics with the finite element approach, one could predict the morphology and mechanical properties of a given assembled nanocomposite. Meanwhile, the development of robust modeling methods

that capture effects of the nanoparticle's structural anisotropy could enable the construction of superstructures with high-level complexity and programmability. Additionally, the identification of descriptors that physically capture the interaction between sub-components could guide the high-throughput assembly of nanoscale building blocks. To this end, machine learning-based artificial intelligence has been employed as a resource-accessible technique for the direct search of physically essential descriptors, thus enabling a fast prediction of structure–property correlation in predesigned superstructures.[269]

With an increasing trend toward nanotechnology commercialization, the ability to successfully translate nanofabrication methods from a laboratory to an industrial setting becomes increasingly important. When compared with top-down lithography-based nanofabrication, bottom-up self-assembly approaches offer obvious advantages, such as low-cost, scalable synthesis, and elimination of complex instrumentation. However, precise control of interparticle spacing and creation of large-scale, defect-free nanoparticle arrays remain formidable challenges and require considerable future effort. Once these issues can be resolved, assembly strategies can be readily implemented into existing manufacturing infrastructure, offering a viable option for next-generation device fabrication.

Conflicts of interest

There are no conflicts to declare.

Acknowledgements

X. G. L. thanks Agency for Science, Technology and Research (A*STAR) under its AME program (Grant No. A1883c0011 and A1983c0038), National Research Foundation, the Prime Minister's Office of Singapore under its NRF Investigatorship Programme (Award No. NRF-NRFI05-2019-0003), the King Abdullah University of Science and Technology (KAUST) Office of Sponsored Research (OSR) under Award No. OSR-2018-CRG7-3736, and National Key R&D Program of China (2019YFC1604605) for supporting this work. X. W. L. thanks the Fundamental Research Funds for the Central Universities (No. 05150-19SH020207).

References

1 G. M. Whitesides and M. Boncheva, *Proc. Natl. Acad. Sci. U. S. A.*, 2002, **99**, 4769–4774.
2 Z. Lu and Y. Yin, *Chem. Soc. Rev.*, 2012, **41**, 6874–6887.
3 Z. Liu, J. Qiao, Z. Niu and Q. Wang, *Chem. Soc. Rev.*, 2012, **41**, 6178–6194.
4 L. Xu, W. Ma, L. Wang, C. Xu, H. Kuang and N. A. Kotov, *Chem. Soc. Rev.*, 2013, **42**, 3114–3126.
5 L. Cademartiri, K. J. M. Bishop, P. W. Snyder and G. A. Ozin, *Philos. Trans. R. Soc., A*, 2012, **370**, 2824–2847.
6 M. A. Boles, M. Engel and D. V. Talapin, *Chem. Rev.*, 2016, **116**, 11220–11289.
7 C. R. Kagan and C. B. Murray, *Nat. Nanotechnol.*, 2015, **10**, 1013–1026.
8 C. Yan and T. Wang, *Chem. Soc. Rev.*, 2017, **46**, 1483–1509.
9 M. Grzelczak, L. M. Liz-Marzán and R. Klajn, *Chem. Soc. Rev.*, 2019, **48**, 1342–1361.
10 B. A. Grzybowski, *Soft Matter*, 2009, **5**, 1109.
11 B. A. Grzybowski, C. E. Wilmer, J. Kim, K. P. Browne and K. J. M. Bishop, *Soft Matter*, 2009, **5**, 1110–1128.
12 M. R. Begley, D. S. Gianola and T. R. Ray, *Science*, 2019, **364**, eaav4299.
13 Q. Q. Shi and W. L. Cheng, *Adv. Funct. Mater.*, 2020, **30**, 1902301.
14 J. Kao, K. Thorkelsson, P. Bai, B. J. Rancatore and T. Xu, *Chem. Soc. Rev.*, 2013, **42**, 2654–2678.
15 K. Kinbara and T. Aida, *Chem. Rev.*, 2005, **105**, 1377–1400.
16 C. Huang, X. Chen, Z. Xue and T. Wang, *Sci. Adv.*, 2020, **6**, eaba1321.
17 P. K. Jain, X. Huang, I. H. El-Sayed and M. A. El-Sayed, *Acc. Chem. Res.*, 2008, **41**, 1578–1586.
18 L. Jiang, X. Chen, N. Lu and L. Chi, *Acc. Chem. Res.*, 2014, **47**, 3009–3017.
19 Y. C. Yang, B. W. Wang, X. D. Shen, L. Y. Yao, L. Wang, X. Chen, S. H. Xie, T. T. Li, J. H. Hu, D. Yang and A. G. Dong, *J. Am. Chem. Soc.*, 2018, **140**, 15038–15047.
20 W. B. Wei, F. Bai and H. Y. Fan, *Angew. Chem., Int. Ed.*, 2019, **58**, 11956–11966.
21 B. Hou, M. Sohn, Y. W. Lee, J. C. Zhang, J. I. Sohn, H. Kim, S. Cha and J. M. Kim, *Nano Energy*, 2019, **62**, 764–771.
22 B. A. Grzybowski, K. Fitzner, J. Paczesny and S. Granick, *Chem. Soc. Rev.*, 2017, **46**, 5647–5678.
23 J. Lee, E. Nakouzi, M. Song, B. Wang, J. Chun and D. Li, *ACS Nano*, 2018, **12**, 12778–12787.
24 S. L. Brown, V. D. Shah, M. V. Morrell, M. Zubich, A. Wagner, A. R. Denton and E. K. Hobbie, *Phys. Rev. E*, 2018, **98**, 062616.
25 T. Wang, D. LaMontagne, J. Lynch, J. Zhuang and Y. C. Cao, *Chem. Soc. Rev.*, 2013, **42**, 2804.
26 L. S. Li and A. P. Alivisatos, *Phys. Rev. Lett.*, 2003, **90**, 097402.
27 J. Gong, G. Li and Z. Tang, *Nano Today*, 2012, **7**, 564–585.
28 Y. Lalatonne, J. Richardi and M. P. Pileni, *Nat. Mater.*, 2004, **3**, 121–125.
29 S. Rong, T. He and P. Zhang, *Appl. Catal., B*, 2020, **267**, 118375.
30 K. J. M. Bishop, C. E. Wilmer, S. Soh and B. A. Grzybowski, *Small*, 2009, **5**, 1600–1630.
31 D. A. Walker, B. Kowalczyk, M. O. de la Cruz and B. A. Grzybowski, *Nanoscale*, 2011, **3**, 1316–1344.
32 J. N. Israelachvili, *Intermolecular and surface forces: revised third edition*, Academic press, 2011.
33 S. Chen, Z. Fan and D. L. Carroll, *J. Phys. Chem. B*, 2002, **106**, 10777–10781.
34 J. Kolny, A. Kornowski and H. Weller, *Nano Lett.*, 2002, **2**, 361–364.
35 A. M. Kalsin, M. Fialkowski, M. Paszewski, S. K. Smoukov, K. J. M. Bishop and B. A. Grzybowski, *Science*, 2006, **312**, 420–424.
36 S. Srivastava, B. Samanta, P. Arumugam, G. Han and V. M. Rotello, *J. Mater. Chem.*, 2007, **17**, 52–55.

37 B. L. V. Prasad, C. M. Sorensen and K. J. Klabunde, *Chem. Soc. Rev.*, 2008, **37**, 1871–1883.
38 G. C. March and D. H. Napper, *J. Colloid Interface Sci.*, 1977, **61**, 383–387.
39 G. S. Grover and S. G. Bike, *Langmuir*, 1995, **11**, 1807–1812.
40 Y. Min, M. Akbulut, K. Kristiansen, Y. Golan and J. Israelachvili, *Nat. Mater.*, 2008, **7**, 527–538.
41 B. D. Korth, P. Keng, I. Shim, S. E. Bowles, C. Tang, T. Kowalewski, K. W. Nebesny and J. Pyun, *J. Am. Chem. Soc.*, 2006, **128**, 6562–6563.
42 D. V. Talapin, E. V. Shevchenko, C. B. Murray, A. V. Titov and P. Král, *Nano Lett.*, 2007, **7**, 1213–1219.
43 R. Klajn, K. J. M. Bishop, M. Fialkowski, M. Paszewski, C. J. Campbell, T. P. Gray and B. A. Grzybowski, *Science*, 2007, **316**, 261–264.
44 A. Manna, P. L. Chen, H. Akiyama, T. X. Wei, K. Tamada and W. Knoll, *Chem. Mater.*, 2003, **15**, 20–28.
45 T. Steiner, *Angew. Chem., Int. Ed.*, 2002, **41**, 48–76.
46 S. R. Johnson, S. D. Evans and R. Brydson, *Langmuir*, 1998, **14**, 6639–6647.
47 Z. Sun, W. Ni, Z. Yang, X. Kou, L. Li and J. Wang, *Small*, 2008, **4**, 1287–1292.
48 L. Etgar, G. Leitus, L. Fradkin, Y. G. Assaraf, R. Tannenbaum and E. Lifshitz, *ChemPhysChem*, 2009, **10**, 2235–2241.
49 D. Baranov, A. Fiore, M. van Huis, C. Giannini, A. Falqui, U. Lafont, H. Zandbergen, M. Zanella, R. Cingolani and L. Manna, *Nano Lett.*, 2010, **10**, 743–749.
50 M. Zanella, G. Bertoni, I. R. Franchini, R. Brescia, D. Baranov and L. Manna, *Chem. Commun.*, 2011, **47**, 203–205.
51 P. Bolhuis and D. Frenkel, *Phys. Rev. Lett.*, 1994, **72**, 2211–2214.
52 G. H. Koenderink, G. A. Vliegenthart, S. G. J. M. Kluijtmans, A. van Blaaderen, A. P. Philipse and H. N. W. Lekkerkerker, *Langmuir*, 1999, **15**, 4693–4696.
53 D. Wang, M. J. A. Hore, X. Ye, C. Zheng, C. B. Murray and R. J. Composto, *Soft Matter*, 2014, **10**, 3404–3413.
54 J. L. Baker, A. Widmer-Cooper, M. F. Toney, P. L. Geissler and A. P. Alivisatos, *Nano Lett.*, 2009, **10**, 195–201.
55 M. Grzelczak, J. Perez-Juste, P. Mulvaney and L. M. Liz-Marzan, *Chem. Soc. Rev.*, 2008, **37**, 1783–1791.
56 D. Garcia-Lojo, S. Nunez-Sanchez, S. Gomez-Grana, M. Grzelczak, I. Pastoriza-Santos, J. Perez-Juste and L. M. Liz-Marzan, *Acc. Chem. Res.*, 2019, **52**, 1855–1864.
57 L. Vigderman, B. P. Khanal and E. R. Zubarev, *Adv. Mater.*, 2012, **24**, 4811–4841.
58 A. Klinkova, R. M. Choueiri and E. Kumacheva, *Chem. Soc. Rev.*, 2014, **43**, 3976–3991.
59 Z. Nie, D. Fava, E. Kumacheva, S. Zou, G. C. Walker and M. Rubinstein, *Nat. Mater.*, 2007, **6**, 609–614.
60 H. Xia, G. Su and D. Wang, *Angew. Chem., Int. Ed.*, 2013, **52**, 3726–3730.
61 B. Han, Z. Zhu, Z. Li, W. Zhang and Z. Tang, *J. Am. Chem. Soc.*, 2014, **136**, 16104–16107.
62 L. Wang, Y. Zhu, L. Xu, W. Chen, H. Kuang, L. Liu, A. Agarwal, C. Xu and N. A. Kotov, *Angew. Chem., Int. Ed.*, 2010, **49**, 5472–5475.
63 C. A. Mirkin, R. L. Letsinger, R. C. Mucic and J. J. Storhoff, *Nature*, 1996, **382**, 607–609.
64 M. R. Jones, R. J. Macfarlane, B. Lee, J. Zhang, K. L. Young, A. J. Senesi and C. A. Mirkin, *Nat. Mater.*, 2010, **9**, 913–917.
65 S. Y. Park, A. K. R. Lytton-Jean, B. Lee, S. Weigand, G. C. Schatz and C. A. Mirkin, *Nature*, 2008, **451**, 553–556.
66 S. J. Tan, M. J. Campolongo, D. Luo and W. Cheng, *Nat. Nanotechnol.*, 2011, **6**, 268–276.
67 W. Cheng, M. J. Campolongo, J. J. Cha, S. J. Tan, C. C. Umbach, D. A. Muller and D. Luo, *Nat. Mater.*, 2009, **8**, 519–525.
68 L. Xu, H. Kuang, C. Xu, W. Ma, L. Wang and N. A. Kotov, *J. Am. Chem. Soc.*, 2011, **134**, 1699–1709.
69 A. J. Mastroianni, S. A. Claridge and A. P. Alivisatos, *J. Am. Chem. Soc.*, 2009, **131**, 8455–8459.
70 S. Vial, D. Nykypanchuk, K. G. Yager, A. V. Tkachenko and O. Gang, *ACS Nano*, 2013, **7**, 5437–5445.
71 M. R. Jones, K. D. Osberg, R. J. Macfarlane, M. R. Langille and C. A. Mirkin, *Chem. Rev.*, 2011, **111**, 3736–3827.
72 S. Srivastava, D. Nykypanchuk, M. Fukuto, J. D. Halverson, A. V. Tkachenko, K. G. Yager and O. Gang, *J. Am. Chem. Soc.*, 2014, **136**, 8323–8332.
73 A. Kuzyk, R. Schreiber, Z. Fan, G. Pardatscher, E.-M. Roller, A. Hogele, F. C. Simmel, A. O. Govorov and T. Liedl, *Nature*, 2012, **483**, 311–314.
74 S. V. Kershaw, A. S. Susha and A. L. Rogach, *Chem. Soc. Rev.*, 2013, **42**, 3033–3087.
75 J. Y. Kim and N. A. Kotov, *Chem. Mater.*, 2013, **26**, 134–152.
76 M. V. Kovalenko and M. I. Bodnarchuk, *Chimia*, 2017, **71**, 461–470.
77 A. Henglein, *Ber. Bunsen-Ges.*, 1982, **86**, 301–305.
78 A. Fojtik, H. Weller, U. Koch and A. Henglein, *Ber. Bunsen-Ges. Phys. Chem.*, 1984, **88**, 969–977.
79 K. Whitham, J. Yang, B. H. Savitzky, L. F. Kourkoutis, F. Wise and T. Hanrath, *Nat. Mater.*, 2016, **15**, 557–563.
80 C. R. Kagan, E. Lifshitz, E. H. Sargent and D. V. Talapin, *Science*, 2016, **353**, aac5523.
81 G. Raino, M. A. Becker, M. I. Bodnarchuk, R. F. Mahrt, M. V. Kovalenko and T. Stoferle, *Nature*, 2018, **563**, 671–675.
82 Y. Xia, T. D. Nguyen, M. Yang, B. Lee, A. Santos, P. Podsiadlo, Z. Tang, S. C. Glotzer and N. A. Kotov, *Nat. Nanotechnol.*, 2011, **6**, 580–587.
83 L. Wang, L. Xu, H. Kuang, C. Xu and N. A. Kotov, *Acc. Chem. Res.*, 2012, **45**, 1916–1926.
84 N. Pradhan, H. Xu and X. Peng, *Nano Lett.*, 2006, **6**, 720–724.
85 Z. Tang, N. A. Kotov and M. Giersig, *Science*, 2002, **297**, 237–240.
86 W. K. Koh, A. C. Bartnik, F. W. Wise and C. B. Murray, *J. Am. Chem. Soc.*, 2010, **132**, 3909–3913.
87 C. O'Sullivan, R. D. Gunning, A. Sanyal, C. A. Barrett, H. Geaney, F. R. Laffir, S. Ahmed and K. M. Ryan, *J. Am. Chem. Soc.*, 2009, **131**, 12250–12257.
88 X. Y. Kong, Y. Ding, R. Yang and Z. L. Wang, *Science*, 2004, **303**, 1348–1351.

89 S. Ithurria, M. D. Tessier, B. Mahler, R. P. S. M. Lobo, B. Dubertret and A. L. Efros, *Nat. Mater.*, 2011, **10**, 936–941.
90 S. Ithurria, G. Bousquet and B. Dubertret, *J. Am. Chem. Soc.*, 2011, **133**, 3070–3077.
91 C. Schliehe, B. H. Juarez, M. Pelletier, S. Jander, D. Greshnykh, M. Nagel, A. Meyer, S. Foerster, A. Kornowski, C. Klinke and H. Weller, *Science*, 2010, **329**, 550–553.
92 S. Srivastava, A. Santos, K. Critchley, K.-S. Kim, P. Podsiadlo, K. Sun, J. Lee, C. Xu, G. D. Lilly, S. C. Glotzer and N. A. Kotov, *Science*, 2010, **327**, 1355–1359.
93 G. Jia, A. Sitt, G. B. Hitin, I. Hadar, Y. Bekenstein, Y. Amit, I. Popov and U. Banin, *Nat. Mater.*, 2014, **13**, 301–307.
94 K.-S. Cho, D. V. Talapin, W. Gaschler and C. B. Murray, *J. Am. Chem. Soc.*, 2005, **127**, 7140–7147.
95 Z. Tang, Z. Zhang, Y. Wang, S. C. Glotzer and N. A. Kotov, *Science*, 2006, **314**, 274–278.
96 B. Yeom and N. A. Kotov, *Nat. Mater.*, 2014, **13**, 228–229.
97 S. Mazzotti, F. Giberti and G. Galli, *Nano Lett.*, 2019, **19**, 3912–3917.
98 F. Bai, D. Wang, Z. Huo, W. Chen, L. Liu, X. Liang, C. Chen, X. Wang, Q. Peng and Y. Li, *Angew. Chem., Int. Ed.*, 2007, **46**, 6650–6653.
99 J. Zhuang, A. D. Shaller, J. Lynch, H. Wu, O. Chen, A. D. Q. Li and Y. C. Cao, *J. Am. Chem. Soc.*, 2009, **131**, 6084–6085.
100 T. Wang, J. Zhuang, J. Lynch, O. Chen, Z. Wang, X. Wang, D. LaMontagne, H. Wu, Z. Wang and Y. C. Cao, *Science*, 2012, **338**, 358–363.
101 T. Wang, X. Wang, D. LaMontagne, Z. Wang and Y. C. Cao, *J. Am. Chem. Soc.*, 2013, **135**, 6022–6025.
102 C. B. Murray, C. R. Kagan and M. G. Bawendi, *Science*, 1995, **270**, 1335–1338.
103 C. R. Kagan, C. B. Murray and M. G. Bawendi, *Phys. Rev. B: Condens. Matter Mater. Phys.*, 1996, **54**, 8633–8643.
104 X. M. Lin, H. M. Jaeger, C. M. Sorensen and K. J. Klabunde, *J. Phys. Chem. B*, 2001, **105**, 3353–3357.
105 W. H. Evers, B. D. Nijs, L. Filion, S. Castillo, M. Dijkstra and D. Vanmaekelbergh, *Nano Lett.*, 2010, **10**, 4235–4241.
106 F. X. Redl, K. S. Cho, C. B. Murray and S. O'Brien, *Nature*, 2003, **423**, 968–971.
107 R. Li, K. Bian, T. Hanrath, W. A. Bassett and Z. Wang, *J. Am. Chem. Soc.*, 2014, **136**, 12047–12055.
108 Z. P. Lv, M. Kapuscinski and L. Bergstrom, *Nat. Commun.*, 2019, **10**, 12.
109 Y. Nagaoka, R. Tan, R. P. Li, H. Zhu, D. Eggert, Y. M. A. Wu, Y. Z. Liu, Z. W. Wang and O. Chen, *Nature*, 2018, **561**, 378–382.
110 E. V. Shevchenko, D. V. Talapin, S. O'Brien and C. B. Murray, *J. Am. Chem. Soc.*, 2005, **127**, 8741–8747.
111 E. V. Shevchenko, D. V. Talapin, N. A. Kotov, S. O'Brien and C. B. Murray, *Nature*, 2006, **439**, 55–59.
112 E. V. Shevchenko, D. V. Talapin, C. B. Murray and S. O'Brien, *J. Am. Chem. Soc.*, 2006, **128**, 3620–3637.
113 K. Overgaag, W. Evers, B. de Nijs, R. Koole, J. Meeldijk and D. Vanmaekelbergh, *J. Am. Chem. Soc.*, 2008, **130**, 7833–7835.
114 H. Friedrich, C. J. Gommes, K. Overgaag, J. D. Meeldijk, W. H. Evers, B. d. Nijs, M. P. Boneschanscher, P. E. de Jongh, A. J. Verkleij, K. P. de Jong, A. van Blaaderen and D. Vanmaekelbergh, *Nano Lett.*, 2009, **9**, 2719–2724.
115 J. J. Urban, D. V. Talapin, E. V. Shevchenko and C. B. Murray, *J. Am. Chem. Soc.*, 2006, **128**, 3248–3255.
116 T. Hanrath, J. J. Choi and D. M. Smilgies, *ACS Nano*, 2009, **3**, 2975–2988.
117 B. Abécassis, M. D. Tessier, P. Davidson and B. Dubertret, *Nano Lett.*, 2013, **14**, 710–715.
118 N. Zhao, K. Liu, J. Greener, Z. Nie and E. Kumacheva, *Nano Lett.*, 2009, **9**, 3077–3081.
119 F. Li, W. C. Yoo, M. B. Beernink and A. Stein, *J. Am. Chem. Soc.*, 2009, **131**, 18548–18555.
120 K. Miszta, J. de Graaf, G. Bertoni, D. Dorfs, R. Brescia, S. Marras, L. Ceseracciu, R. Cingolani, R. van Roij, M. Dijkstra and L. Manna, *Nat. Mater.*, 2011, **10**, 872–876.
121 H. Li, A. G. Kanaras and L. Manna, *Acc. Chem. Res.*, 2013, **46**, 1387–1396.
122 A. Castelli, J. de Graaf, S. Marras, R. Brescia, L. Goldoni, L. Manna and M. P. Arciniegas, *Nat. Commun.*, 2018, **9**, 1141.
123 W. Qi, J. d. Graaf, F. Qiao, S. Marras, L. Manna and M. Dijkstra, *Nano Lett.*, 2012, **12**, 5299–5303.
124 L. Ceseracciu, K. Miszta, F. De Angelis, S. Marras, M. Prato, R. Brescia, A. Scarpellini and L. Manna, *Nanoscale*, 2013, **5**, 681–686.
125 M. A. Boles and D. V. Talapin, *ACS Nano*, 2019, **13**, 5375–5384.
126 M. A. Kostiainen, P. Hiekkataipale, A. Laiho, V. Lemieux, J. Seitsonen, J. Ruokolainen and P. Ceci, *Nat. Nanotechnol.*, 2013, **8**, 52–56.
127 D. V. Talapin, E. V. Shevchenko, M. I. Bodnarchuk, X. Ye, J. Chen and C. B. Murray, *Nature*, 2009, **461**, 964–967.
128 A. Dong, J. Chen, P. M. Vora, J. M. Kikkawa and C. B. Murray, *Nature*, 2010, **466**, 474–477.
129 Y. Kang, X. Ye, J. Chen, L. Qi, R. E. Diaz, V. Doan-Nguyen, G. Xing, C. R. Kagan, J. Li, R. J. Gorte, E. A. Stach and C. B. Murray, *J. Am. Chem. Soc.*, 2013, **135**, 1499–1505.
130 S. L. Tripp, R. E. Dunin-Borkowski and A. Wei, *Angew. Chem., Int. Ed.*, 2003, **42**, 5591–5593.
131 S. L. Tripp, S. V. Pusztay, A. E. Ribbe and A. Wei, *J. Am. Chem. Soc.*, 2002, **124**, 7914–7915.
132 P. Y. Keng, I. Shim, B. D. Korth, J. F. Douglas and J. Pyun, *ACS Nano*, 2007, **1**, 279–292.
133 R. Rosensweig, *Ferrohydrodynamics*, Cambridge University Press, Cambridge, 1985.
134 K. Butter, P. H. H. Bomans, P. M. Frederik, G. J. Vroege and A. P. Philipse, *Nat. Mater.*, 2003, **2**, 88–91.
135 M. Klokkenburg, C. Vonk, E. M. Claesson, J. D. Meeldijk, B. H. Erné and A. P. Philipse, *J. Am. Chem. Soc.*, 2004, **126**, 16706–16707.
136 J. J. Benkoski, S. E. Bowles, B. D. Korth, R. L. Jones, J. F. Douglas, A. Karim and J. Pyun, *J. Am. Chem. Soc.*, 2007, **129**, 6291–6297.
137 C. B. Murray, S. Sun, W. Gaschler, H. Doyle, T. A. Betley and C. R. Kagan, *IBM J. Res. Dev.*, 2001, **45**, 47–56.

138 A. Ahniyaz, Y. Sakamoto and L. Bergström, *Proc. Natl. Acad. Sci. U. S. A.*, 2007, **104**, 17570–17574.
139 J. Ge, Y. Hu and Y. Yin, *Angew. Chem., Int. Ed.*, 2007, **46**, 7428–7431.
140 J. Ge, L. He, J. Goebl and Y. Yin, *J. Am. Chem. Soc.*, 2009, **131**, 3484–3486.
141 J. Bibette, *J. Magn. Magn. Mater.*, 1993, **122**, 37–41.
142 F. L. Calderon, T. Stora, O. Mondain Monval, P. Poulin and J. Bibette, *Phys. Rev. Lett.*, 1994, **72**, 2959–2962.
143 H. Kim, J. Ge, J. Kim, S. E. Choi, H. Lee, H. Lee, W. Park, Y. Yin and S. Kwon, *Nat. Photonics*, 2009, **3**, 534–540.
144 J. Ge and Y. Yin, *Angew. Chem., Int. Ed.*, 2011, **50**, 1492–1522.
145 W. H. Chong, L. K. Chin, R. L. S. Tan, H. Wang, A. Q. Liu and H. Chen, *Angew. Chem., Int. Ed.*, 2013, **52**, 8570–8573.
146 J. Ge, H. Lee, L. He, J. Kim, Z. Lu, H. Kim, J. Goebl, S. Kwon and Y. Yin, *J. Am. Chem. Soc.*, 2009, **131**, 15687–15694.
147 G. Singh, H. Chan, A. Baskin, E. Gelman, N. Repnin, P. Král and R. Klajn, *Science*, 2014, **345**, 1149–1153.
148 R. M. Erb, H. S. Son, B. Samanta, V. M. Rotello and B. B. Yellen, *Nature*, 2009, **457**, 999–1002.
149 S. Sacanna, L. Rossi and D. J. Pine, *J. Am. Chem. Soc.*, 2012, **134**, 6112–6115.
150 J. Yan, M. Bloom, S. C. Bae, E. Luijten and S. Granick, *Nature*, 2012, **491**, 578–581.
151 D. Zerrouki, J. Baudry, D. Pine, P. Chaikin and J. Bibette, *Nature*, 2008, **455**, 380–382.
152 L. He, M. Wang, Q. Zhang, Y. Lu and Y. Yin, *Nano Lett.*, 2012, **13**, 264–271.
153 R. Dreyfus, J. Baudry, M. L. Roper, M. Fermigier, H. A. Stone and J. Bibette, *Nature*, 2005, **437**, 862–865.
154 L. Zhang, J. J. Abbott, L. Dong, B. E. Kratochvil, D. Bell and B. J. Nelson, *Appl. Phys. Lett.*, 2009, **94**, 064107.
155 B. A. Evans, A. R. Shields, R. L. Carroll, S. Washburn, M. R. Falvo and R. Superfine, *Nano Lett.*, 2007, **7**, 1428–1434.
156 M. Vilfan, A. Potočnik, B. Kavčič, N. Osterman, I. Poberaj, A. Vilfan and D. Babič, *Proc. Natl. Acad. Sci. U. S. A.*, 2010, **107**, 1844–1847.
157 A. Snezhko and I. S. Aranson, *Nat. Mater.*, 2011, **10**, 698–703.
158 F. Wang, R. Deng, J. Wang, Q. Wang, Y. Han, H. Zhu, X. Chen and X. Liu, *Nat. Mater.*, 2011, **10**, 968–973.
159 F. Wang and X. Liu, *Chem. Soc. Rev.*, 2009, **38**, 976–989.
160 Y. Wang, K. Zheng, S. Song, D. Fan, H. Zhang and X. Liu, *Chem. Soc. Rev.*, 2018, **47**, 6473–6485.
161 L. Liang, X. Qin, K. Zheng and X. Liu, *Acc. Chem. Res.*, 2019, **52**, 228–236.
162 Q. Liu, Y. Sun, C. Li, J. Zhou, C. Li, T. Yang, X. Zhang, T. Yi, D. Wu and F. Li, *ACS Nano*, 2011, **5**, 3146–3157.
163 Y. Bao, Q. A. N. Luu, C. Lin, J. M. Schloss, P. S. May and C. Jiang, *J. Mater. Chem.*, 2010, **20**, 8356–8361.
164 J. Liu and Y. D. Li, *Adv. Mater.*, 2007, **19**, 1118–1122.
165 P. Li, Q. Peng and Y. Li, *Adv. Mater.*, 2009, **21**, 1945–1948.
166 Q. Zhang, X. Wang and Y. Zhu, *J. Mater. Chem.*, 2011, **21**, 12132–12138.
167 R. Si, Y. W. Zhang, H. P. Zhou, L. D. Sun and C. H. Yan, *Chem. Mater.*, 2006, **19**, 18–27.
168 Y. W. Zhang, X. Sun, R. Si, L. P. You and C. H. Yan, *J. Am. Chem. Soc.*, 2005, **127**, 3260–3261.
169 Y. Ding, J. Gu, J. Ke, Y.-W. Zhang and C.-H. Yan, *Angew. Chem., Int. Ed.*, 2011, **50**, 12330–12334.
170 Y. P. Du, Y. W. Zhang, L. D. Sun and C. H. Yan, *J. Am. Chem. Soc.*, 2009, **131**, 3162–3163.
171 T. Paik, D. K. Ko, T. R. Gordon, V. Doan-Nguyen and C. B. Murray, *ACS Nano*, 2011, **5**, 8322–8330.
172 T. Paik, T. R. Gordon, A. M. Prantner, H. Yun and C. B. Murray, *ACS Nano*, 2013, **7**, 2850–2859.
173 T. Paik and C. B. Murray, *Nano Lett.*, 2013, **13**, 2952–2956.
174 X. Ye, J. E. Collins, Y. Kang, J. Chen, D. T. N. Chen, A. G. Yodh and C. B. Murray, *Proc. Natl. Acad. Sci. U. S. A.*, 2010, **107**, 22430–22435.
175 X. Ye, J. Chen, M. Engel, J. A. Millan, W. Li, L. Qi, G. Xing, J. E. Collins, C. R. Kagan, J. Li, S. C. Glotzer and C. B. Murray, *Nat. Chem.*, 2013, **5**, 466–473.
176 L.-L. Li and Y. Lu, *J. Am. Chem. Soc.*, 2015, **137**, 5272–5275.
177 L.-L. Li, P. Wu, K. Hwang and Y. Lu, *J. Am. Chem. Soc.*, 2013, **135**, 2411–2414.
178 H. Ge, D. Wang, Y. Pan, Y. Guo, H. Li, F. Zhang, X. Zhu, Y. Li, C. Zhang and L. Huang, *Angew. Chem., Int. Ed.*, 2020, **59**, 8133–8137.
179 S. Li, L. Xu, W. Ma, X. Wu, M. Sun, H. Kuang, L. Wang, N. A. Kotov and C. Xu, *J. Am. Chem. Soc.*, 2016, **138**, 306–312.
180 N. J. Halas, S. Lal, W. S. Chang, S. Link and P. Nordlander, *Chem. Rev.*, 2011, **111**, 3913–3961.
181 L. M. Liz-Marzán, *Langmuir*, 2005, **22**, 32–41.
182 M. Yang, G. Chen, Y. Zhao, G. Silber, Y. Wang, S. Xing, Y. Han and H. Chen, *Phys. Chem. Chem. Phys.*, 2010, **12**, 11850–11860.
183 M. A. Correa-Duarte, J. Pérez-Juste, A. Sánchez-Iglesias, M. Giersig and L. M. Liz-Marzán, *Angew. Chem., Int. Ed.*, 2005, **44**, 4375–4378.
184 C. Tabor, D. Van Haute and M. A. El-Sayed, *ACS Nano*, 2009, **3**, 3670–3678.
185 P. Pramod and K. G. Thomas, *Adv. Mater.*, 2008, **20**, 4300–4305.
186 G. Mie, *Ann. Phys.*, 1908, **330**, 377–445.
187 S. Sheikholeslami, Y.-w. Jun, P. K. Jain and A. P. Alivisatos, *Nano Lett.*, 2010, **10**, 2655–2660.
188 P. K. Jain, S. Eustis and M. A. El-Sayed, *J. Phys. Chem. B*, 2006, **110**, 18243–18253.
189 L. Chuntonov and G. Haran, *Nano Lett.*, 2011, **11**, 2440–2445.
190 H. Wang, D. W. Brandl, P. Nordlander and N. J. Halas, *Acc. Chem. Res.*, 2007, **40**, 53–62.
191 C. Radloff and N. J. Halas, *Nano Lett.*, 2004, **4**, 1323–1327.
192 R. Bardhan, S. Mukherjee, N. A. Mirin, S. D. Levit, P. Nordlander and N. J. Halas, *J. Phys. Chem. C*, 2010, **114**, 7378–7383.
193 R. Bardhan, N. K. Grady, T. Ali and N. J. Halas, *ACS Nano*, 2010, **4**, 6169–6179.

194 T. Taniguchi and K. Monde, *J. Am. Chem. Soc.*, 2012, **134**, 3695–3698.
195 J. M. Slocik, A. O. Govorov and R. R. Naik, *Nano Lett.*, 2011, **11**, 701–705.
196 A. O. Govorov, *J. Phys. Chem. C*, 2011, **115**, 7914–7923.
197 Y. Xia, Y. Zhou and Z. Tang, *Nanoscale*, 2011, **3**, 1374–1382.
198 A. O. Govorov, Y. K. Gun'ko, J. M. Slocik, V. A. Gerard, Z. Fan and R. R. Naik, *J. Mater. Chem.*, 2011, **21**, 16806–16818.
199 A. Guerrero-Martínez, B. Auguié, J. L. Alonso-Gómez, Z. Džolić, S. Gómez-Graña, M. Žinić, M. M. Cid and L. M. Liz-Marzán, *Angew. Chem., Int. Ed.*, 2011, **50**, 5499–5503.
200 S. H. Jung, J. Jeon, H. Kim, J. Jaworski and J. H. Jung, *J. Am. Chem. Soc.*, 2014, **136**, 6446–6452.
201 J. George and K. G. Thomas, *J. Am. Chem. Soc.*, 2010, **132**, 2502–2503.
202 A. Inoue, M. Fujii, H. Sugimoto and K. Imakita, *J. Phys. Chem. C*, 2015, **119**, 25108–25113.
203 B. Demory, T. A. Hill, C. H. Teng, L. Zhang, H. Deng and P. C. Ku, *ACS Photonics*, 2015, **2**, 1065–1070.
204 E. Cohen-Hoshen, G. W. Bryant, I. Pinkas, J. Sperling and I. Bar-Joseph, *Nano Lett.*, 2012, **12**, 4260–4264.
205 E. V. Shevchenko, M. Ringler, A. Schwemer, D. V. Talapin, T. A. Klar, A. L. Rogach, J. Feldmann and A. P. Alivisatos, *J. Am. Chem. Soc.*, 2008, **130**, 3274–3275.
206 J. Lee, P. Hernandez, J. Lee, A. O. Govorov and N. A. Kotov, *Nat. Mater.*, 2007, **6**, 291–295.
207 C. Zhou, Y. Zhong, H. Dong, W. Zheng, J. Tan, Q. Jie, A. Pan, L. Zhang and W. Xie, *Nat. Commun.*, 2020, **11**, 329.
208 D. Baranov, S. Toso, M. Imran and L. Manna, *J. Phys. Chem. Lett.*, 2019, **10**, 655–660.
209 M. Corricelli, F. Enrichi, D. Altamura, L. De Caro, C. Giannini, A. Falqui, A. Agostiano, M. L. Curri and M. Striccoli, *J. Phys. Chem. C*, 2012, **116**, 6143–6152.
210 S. W. Clark, J. M. Harbold and F. W. Wise, *J. Phys. Chem. C*, 2007, **111**, 7302–7305.
211 A. Sukhanova, A. V. Baranov, T. S. Perova, J. H. M. Cohen and I. Nabiev, *Angew. Chem., Int. Ed.*, 2006, **45**, 2048–2052.
212 C. Bernardo, I. Moura, Y. N. Fernández, E. J. Nunes-Pereira, P. J. G. Coutinho, A. M. F. Garcia, P. Schellenberg, M. Belsley, M. F. Costa, T. Stauber and M. I. Vasilevskiy, *J. Phys. Chem. C*, 2014, **118**, 4982–4990.
213 T. Förster, *Ann. Phys.*, 1948, **437**, 55–75.
214 C. Kagan, C. Murray, M. Nirmal and M. Bawendi, *Phys. Rev. Lett.*, 1996, **76**, 1517–1520.
215 L. Guo, T. D. Krauss, C. B. Poitras, M. Lipson, X. Teng and H. Yang, *Appl. Phys. Lett.*, 2006, **89**, 061104.
216 S. Crooker, J. Hollingsworth, S. Tretiak and V. Klimov, *Phys. Rev. Lett.*, 2002, **89**, 186802.
217 T. Franzl, A. Shavel, A. L. Rogach, N. Gaponik, T. A. Klar, A. Eychmüller and J. Feldmann, *Small*, 2005, **1**, 392–395.
218 T. Franzl, T. A. Klar, S. Schietinger, A. L. Rogach and J. Feldmann, *Nano Lett.*, 2004, **4**, 1599–1603.
219 T. A. Klar, T. Franzl, A. L. Rogach and J. Feldmann, *Adv. Mater.*, 2005, **17**, 769–773.
220 A. H. Lu, E. L. Salabas and F. Schüth, *Angew. Chem., Int. Ed.*, 2007, **46**, 1222–1244.
221 S. Laurent, D. Forge, M. Port, A. Roch, C. Robic, L. Vander Elst and R. N. Muller, *Chem. Rev.*, 2008, **108**, 2064–2110.
222 Q. Dai and A. Nelson, *Chem. Soc. Rev.*, 2010, **39**, 4057–4066.
223 S. Singamaneni, V. N. Bliznyuk, C. Binek and E. Y. Tsymbal, *J. Mater. Chem.*, 2011, **21**, 16819–16845.
224 M. Colombo, S. Carregal-Romero, M. F. Casula, L. Gutierrez, M. P. Morales, I. B. Bohm, J. T. Heverhagen, D. Prosperi and W. J. Parak, *Chem. Soc. Rev.*, 2012, **41**, 4306–4334.
225 I. Lisiecki, C. Salzemann, D. Parker, P.-A. Albouy and M.-P. Pileni, *J. Phys. Chem. C*, 2007, **111**, 12625–12631.
226 D. Parker, I. Lisiecki, C. Salzemann and M.-P. Pileni, *J. Phys. Chem. C*, 2007, **111**, 12632–12638.
227 M. P. Pileni, *Acc. Chem. Res.*, 2007, **40**, 685–693.
228 M. P. Pileni, *Acc. Chem. Res.*, 2008, **41**, 1799–1809.
229 I. Lisiecki, D. Parker, C. Salzemann and M. P. Pileni, *Chem. Mater.*, 2007, **19**, 4030–4036.
230 J. Chen, A. Dong, J. Cai, X. Ye, Y. Kang, J. M. Kikkawa and C. B. Murray, *Nano Lett.*, 2010, **10**, 5103–5108.
231 M. Cargnello, A. C. Johnston-Peck, B. T. Diroll, E. Wong, B. Datta, D. Damodhar, V. V. T. Doan-Nguyen, A. A. Herzing, C. R. Kagan and C. B. Murray, *Nature*, 2015, **524**, 450–453.
232 R. Elghanian, J. J. Storhoff, R. C. Mucic, R. L. Letsinger and C. A. Mirkin, *Science*, 1997, **277**, 1078–1081.
233 F. Xia, X. L. Zuo, R. Q. Yang, Y. Xiao, D. Kang, A. Vallee-Belisle, X. Gong, J. D. Yuen, B. B. Y. Hsu, A. J. Heeger and K. W. Plaxco, *Proc. Natl. Acad. Sci. U. S. A.*, 2010, **107**, 10837–10841.
234 C. Sonnichsen, B. M. Reinhard, J. Liphardt and A. P. Alivisatos, *Nat. Biotechnol.*, 2005, **23**, 741–745.
235 E. Le Ru and P. Etchegoin, *Principles of Surface-Enhanced Raman Spectroscopy: and related plasmonic effects*, Elsevier, 2008.
236 D. K. Lim, K. S. Jeon, H. M. Kim, J.-M. Nam and Y. D. Suh, *Nat. Mater.*, 2010, **9**, 60–67.
237 Z. Zhu, H. Meng, W. Liu, X. Liu, J. Gong, X. Qiu, L. Jiang, D. Wang and Z. Tang, *Angew. Chem.*, 2011, **123**, 1631–1634.
238 Y. Xia, L. Song and C. Zhu, *Anal. Chem.*, 2011, **83**, 1401–1407.
239 Z. Li, Z. Zhu, W. Liu, Y. Zhou, B. Han, Y. Gao and Z. Tang, *J. Am. Chem. Soc.*, 2012, **134**, 3322–3325.
240 T. Hu, B. P. Isaacoff, J. H. Bahng, C. Hao, Y. Zhou, J. Zhu, X. Li, Z. Wang, S. Liu, C. Xu, J. S. Biteen and N. A. Kotov, *Nano Lett.*, 2014, **14**, 6799–6810.
241 Z. Zhu, W. Liu, Z. Li, B. Han, Y. Zhou, Y. Gao and Z. Tang, *ACS Nano*, 2012, **6**, 2326–2332.
242 J. Song, J. Zhou and H. Duan, *J. Am. Chem. Soc.*, 2012, **134**, 13458–13469.
243 V. Shanmugam, S. Selvakumar and C.-S. Yeh, *Chem. Soc. Rev.*, 2014, **43**, 6254–6287.
244 L. Nie and X. Chen, *Chem. Soc. Rev.*, 2014, **43**, 7132–7170.
245 L. Cheng, C. Wang, L. Feng, K. Yang and Z. Liu, *Chem. Rev.*, 2014, **114**, 10869–10939.

246 S. Mura, J. Nicolas and P. Couvreur, *Nat. Mater.*, 2013, **12**, 991–1003.
247 Z. Xiao, C. Ji, J. Shi, E. M. Pridgen, J. Frieder, J. Wu and O. C. Farokhzad, *Angew. Chem., Int. Ed.*, 2012, **51**, 11853–11857.
248 J. Lin, S. Wang, P. Huang, Z. Wang, S. Chen, G. Niu, W. Li, J. He, D. Cui, G. Lu, X. Chen and Z. Nie, *ACS Nano*, 2013, **7**, 5320–5329.
249 P. Huang, J. Lin, W. Li, P. Rong, Z. Wang, S. Wang, X. Wang, X. Sun, M. Aronova, G. Niu, R. D. Leapman, Z. Nie and X. Chen, *Angew. Chem., Int. Ed.*, 2013, **52**, 13958–13964.
250 K. Liu, X. Liu, Q. Zeng, Y. Zhang, L. Tu, T. Liu, X. Kong, Y. Wang, F. Cao, S. A. G. Lambrechts, M. C. G. Aalders and H. Zhang, *ACS Nano*, 2012, **6**, 4054–4062.
251 F. Li, Y. Du, J. Liu, H. Sun, J. Wang, R. Li, D. Kim, T. Hyeon and D. Ling, *Adv. Mater.*, 2018, **30**, 1802808.
252 Y. Feng, Y. Wu, J. Zuo, L. Tu, I. Que, Y. Chang, L. J. Cruz, A. Chan and H. Zhang, *Biomaterials*, 2019, **201**, 33–41.
253 C. Schmidtke, R. Eggers, R. Zierold, A. Feld, H. Kloust, C. Wolter, J. Ostermann, J. P. Merkl, T. Schotten, K. Nielsch and H. Weller, *Langmuir*, 2014, **30**, 11190–11196.
254 J. Guo, W. Yang and C. Wang, *Adv. Mater.*, 2013, **25**, 5196–5214.
255 J. Yang, C. H. Lee, H. J. Ko, J. S. Suh, H. G. Yoon, K. Lee, Y. M. Huh and S. Haam, *Angew. Chem., Int. Ed.*, 2007, **46**, 8836–8839.
256 S. I. Jenkins, M. R. Pickard, N. Granger and D. M. Chari, *ACS Nano*, 2011, **5**, 6527–6538.
257 J. H. Lee, K. J. Chen, S. H. Noh, M. A. Garcia, H. Wang, W. Y. Lin, H. Jeong, B. J. Kong, D. B. Stout, J. Cheon and H. R. Tseng, *Angew. Chem., Int. Ed.*, 2013, **52**, 4384–4388.
258 G. Guo, L. Ji, X. Shen, B. Wang, H. Li, J. Hu, D. Yang and A. Dong, *J. Mater. Chem. A*, 2016, **4**, 16128–16135.
259 O. Chen, L. Riedemann, F. Etoc, H. Herrmann, M. Coppey, M. Barch, C. T. Farrar, J. Zhao, O. T. Bruns, H. Wei, P. Guo, J. Cui, R. Jensen, Y. Chen, D. K. Harris, J. M. Cordero, Z. W. Wang, A. Jasanoff, D. Fukumura, R. Reimer, M. Dahan, R. K. Jain and M. G. Bawendi, *Nat. Commun.*, 2014, **5**, 5093.
260 Y. C. Jiao, D. D. Han, Y. Ding, X. F. Zhang, G. N. Guo, J. H. Hu, D. Yang and A. G. Dong, *Nat. Commun.*, 2015, **6**, 6420.
261 D. J. Milliron, R. Buonsanti, A. Llordes and B. A. Helms, *Acc. Chem. Res.*, 2014, **47**, 236.
262 J. Li, Y. Wang, T. Zhou, H. Zhang, X. Sun, J. Tang, L. Zhang, A. M. Al-Enizi, Z. Yang and G. Zheng, *J. Am. Chem. Soc.*, 2015, **137**, 14305–14312.
263 L. Su, D. Han, G. Zhu, H. Xu, W. Luo, L. Wang, W. Jiang, A. Dong and J. Yang, *Nano Lett.*, 2019, **19**, 5423–5430.
264 Y. Jiao, D. Han, L. Liu, L. Ji, G. Guo, J. Hu, D. Yang and A. Dong, *Angew. Chem., Int. Ed.*, 2015, **54**, 5727–5731.
265 B. Wang, X. Wang, J. Zou, Y. Yan, S. Xie, G. Hu, Y. Li and A. Dong, *Nano Lett.*, 2017, **17**, 2003–2009.
266 T. Li, B. Xue, B. Wang, G. Guo, D. Han, Y. Yan and A. Dong, *J. Am. Chem. Soc.*, 2017, **139**, 12133–12136.
267 Y. Yang, B. Wang, X. Shen, L. Yao, L. Wang, X. Chen, S. Xie, T. Li, J. Hu, D. Yang and A. Dong, *J. Am. Chem. Soc.*, 2018, **140**, 15038–15047.
268 J. Bao, W. Chen, T. Liu, Y. Zhu, P. Jin, L. Wang, J. Liu, Y. Wei and Y. Li, *ACS Nano*, 2007, **1**, 293–298.
269 C. S. Adorf, T. C. Moore, Y. J. U. Melle and S. C. Glotzer, *J. Phys. Chem. B*, 2020, **124**, 69–78.